Escola de Camins
Escola Tècnica Superior d'Enginyeria de Camins, Canals i Ports
UPC BARCELONATECH

TREBALL FINAL DE MÀSTER

Flexural buckling of stainless steel angle columns

Treball realitzat per:

María Fernanda Gouveia

Dirigit per:

Itsaso Arrayago Luquin

Esther Real Saladrigas

Màster en:

Enginyeria Estructural i de la Construcció

Barcelona, Gener 2018

Departament d'Enginyeria Civil i Ambiental

ABSTRACT

Stainless steel is a corrosion and heat resistant material, composed by a minimum of 10.5% chromium, that is being used more often with the pass of the time, thanks to this high corrosion resistant, which makes it very valuable in highly aggressive and corrosive environments. However, in the construction industry it is still not largely used, mainly because of the lack of information about the structural behavior of stainless steel different cross-sections, and therefore the non-efficient structural design governed by the conservative design guides.

An extensive parametric study is carried out in this work, through finite element (FE) models, on six different cross-sections of austenitic, ferritic and duplex stainless steel grades, and nine different member slenderness. The different members are subjected to pure compression in order to study the member behavior by analyzing the obtained numerical results and evaluate the buckling curve codified in EN1993-1-4.

Therefore, this work investigates the member behavior of stainless steel equal-leg angle columns, where the influence of the interaction of flexural buckling with other buckling modes, such as torsional buckling is addressed, and proposes a new buckling curve for the minor axis flexural buckling resistance, due to the conservativeness of the one codified in EN1993-1-4.

This proposal for the minor axis flexural buckling resistance of stainless steel columns with angle sections is validated through a reliability analysis, made according to EN1990.

ACKNOLEDGMENTS

First of all my true and deep gratitude to my tutors Itsaso Arrayago and Professor Esther Real from the Department of Civil and Environmental Engineering at Universitat Politècnica de Catalunya. They were essential during all this process, thanks to their help, knowledge and support this work was possible.

Also thanks to Prof. Enrique Mirambell for his help in some specific doubts and to Prof. Rolando Chacón for his help especially with the software ABAQUS.

Thanks to all my family, especially to my parents, Niuska and Raul, who are my role model and my strength in difficult times, and to Mauricio who has been my support through this process. Without them, it would have been impossible to finish this work.

CONTENTS

ABSTRACT **3**

ACKNOLEDGMENTS **4**

1. INTRODUCTION **8**

1.1 Background 8

1.2 Objectives 9

1.2.1 General objectives 9

1.2.2 Specific objectives 9

1.3 Methodology 9

1.4 Content of the work 10

2. LITERATURE REVIEW **11**

2.1 Stainless steel 11

2.1.1 Types of stainless steel 12

2.1.2 Material response 12

2.1.3 Material models 14

2.1.4 Life cycle cost and environmental impact 15

2.1.5 Structural use 16

2.1.5.1 Use of cold-formed 17

2.1.6 International design standards 17

2.2 Stainless steel open sections 18

2.2.1 Angle sections 18

2.2.3 Cross-section response 20

2.2.3.1 Formulation for cross-sectional resistance 20

2.2.4 Member response in compression 22

2.2.4.1 Previous experimental programmes on angle section members 22

2.2.4.2 Formulation for member resistance 23

2.2.4.3 Flexural buckling 23

2.2.4.4 Torsional and torsional-flexural buckling 25

3. NUMERICAL ANALYSIS: FINITE ELEMENT MODELS **27**

3.1 Introduction 27

3.2 General assumptions 27

3.2.1 Model 27

3.2.2 Steps 28
3.2.3 Mesh 29
3.2.4 Residual stress 29
3.2.5 Initial geometric imperfections 29
3.3 Validation of the numerical models 31
3.3.1 de Menezes et al. Validation model (2017) 31
3.3.2 Lendesmann et al. (2017) validation model 39
3.4 Parametric study 46
3.4.1 Overall slenderness 46
3.4.2 Geometry 47
3.4.3 Material 48
3.4.5 Imperfections 51
3.4.6 Boundary conditions 53

4. BEHAVIOR OF STAINLESS STEEL ANGLE COLUMNS 55
4.1 Analysis 55
4.2 Comparison of the FE results and the Design Guides 59

5. DESIGN PROPOSAL 68
5.1 Proposal 68
5.2 Reliability Analysis 72

6. CONCLUSIONS 77
6.1 Suggestions for future research 78

7. REFERENCES 79

1. INTRODUCTION

1.1 Background

Stainless steel is the name given to a group of materials that are corrosion and heat resistant, composed by a minimum of 10.5% chromium and other alloys elements, such as nickel, titanium, etc. The use of this material is increasing with the pass of the time, thanks to its high corrosion resistant, which makes stainless steel very valuable in highly aggressive and corrosive environments.

In the construction industry, it is still not largely used, mainly because of the lack of information about the structural behavior of stainless steel different cross-sections, and therefore the non-efficient structural design is governed by the conservative design guides. However, its potential in this particular industry is very wide, due to its great properties such as high corrosion and fire resistance, aesthetic appeal, good strength, toughness and fatigue properties. Another important property of this material is its high ductility, which is a determining factor if resistance to seismic actions is required, that is to say in seismic zones. In addition, when the non-linear stress-strain response of the material and strain hardening effects are taken into account the capacity of the structure is improved even more.

Angle sections have been extensively used in various applications because of different reasons, one of them is their wide range of different sizes available (Kettler, 2016). According to Kettler (2016) and Jain (2014) angle sections are used in structural applications especially in members with primary axial forces, because of their relatively simple connections and the simplicity of their fabrication process. Other advantages for the construction industry of this particular section are its compactness, lightness in weight and economic transportation. However its structural behavior is quite complex, mainly because its centroid lies outside the section hindering the application of the forces which tend to act eccentrically causing the rotation of the principal axis. Therefore, steel angle columns show generally two main failure modes, torsional-flexural and flexural buckling.

In addition, recent research works on stainless steel open sections showed that the flexural buckling curves for stainless steel in EN1993-1-4 (2006) are very conservative, and for that reason, they need to be revised.

For these reasons, and in order to gain knowledge as well as extend the limited research about the behavior of open sections, angle sections subjected to pure compression are studied in this work.

To investigate the behavior of stainless steel angle sections a finite element (FE) model has been developed, and validated with experimental data in the literature. Then, parametric studies are carried out to increase the amount of available data, considering 3 different stainless steel grades (Austenitic (1.4301), Duplex (1.4462) and Ferritic (1.4003)), 6 different cross-sections and 9 member slenderness.

1.2 Objectives

The main objectives of this work are to understand the general behavior of stainless steel angle section members when subjected to pure compression and to evaluate the buckling curve addressed in the Eurocode EN1993-1-4 for this section, in order to verify if this curve leads to an efficient design. The objectives, subdivided in general and specific objectives are described in this section.

1.2.1 General objectives

When designing structures is very important to do it efficiently, regardless the considered construction material, in order to reduce costs and environmental impact. However, when the material is stainless steel, efficient design becomes a determining factor, due to its high cost in comparison to carbon steel. With efficient design expressions that account for the non-linear stress-strain response and strain hardening effects, and the use of less conservative buckling curves for stainless steel, a more efficient, economic and sustainable structural design would be achieved. Therefore, this work has been focused towards the main objective of understanding the cross-sections and member behavior of stainless steel angle sections in order to propose alternative guidance. More efficient design methods would lead to less tonnage use of the material for the same applied structural load levels, considerably reducing initial material costs and environmental impact.

1.2.2 Specific objectives

The specific objectives of this work are the following:

- Strengthen the available data on stainless steel angle sections by conducting an extensive numerical research that will allow a better understanding of the behavior of these sections.
- Develop and validate a numerical finite element (FE) model in ABAQUS, in order to perform a parametric study for stainless steel angle sections.
- Develop extensive parametric study on stainless steel angle sections for different
- Evaluation of the buckling curves currently provided for stainless steel equal leg angle sections and proposal of new curves if necessary.
- Perform a reliability analysis in order to validate the proposed curves through statistical analysis.

1.3 Methodology

The methodology to be developed in order to reach all the objectives described in the previous section is briefly presented herein.

1) Literature review. Review of the current research in structural stainless steel, previous experimental programmes and codified design guidance.

2) Finite element model validation: Benchmark. Create and validate a finite element (FE) model of angle sections in ABAQUS, by studying two cases of the literature, and comparing the results of both studies.
3) Parametric study. Validated FE models systematically utilized to identify the influence of the key parameters in the behavior of stainless steel cross-sections and elements.
4) Analysis of the member behavior of stainless steel equal leg angle sections subjected to pure compression. Evaluation of the buckling curves currently provided for stainless steel open sections and proposal of new curves if necessary. Reliability of the new proposal demonstrated according to Annex D of EN1990 (2005).

1.4 Content of the work

In this first chapter a brief introduction is presented, then the research objectives of the study are specified and the methodology of the work is described. Finally the content of the work is provided.

In chapter 2 a brief review of the literature that is relevant to this work is presented, especially about the material, the description of the different models for its non-linear stress-strain behavior, and its applications in the construction industry. A summary of the existing design standards is also presented. And finally a brief compilation of previous studies in angle sections and the provided expressions in EN1993-1-4 (2006) for design are shown.

Chapter 3 contains all the information regarding the finite element (FE) analyses conducted in this work using the general-purpose software ABAQUS, the general assumptions, the validation of the models against experimental (literature) results, and the details of the conducted parametric study,

The analysis of the results is presented in chapter 4, where a comprehensive study on the member behavior of stainless steel angle sections subjected to pure compression is shown, based on the numerical data obtained through the parametric study. The provided buckling curve in EN1993-1-4 is evaluated.

In chapter 5 a design proposal is made, consisting in a different buckling curve for stainless steel angle sections than the one presented in EN1993-1-4. Later, a reliability analysis is made in order to validate this proposal.

Chapter 6 contains the conclusions of his research work, as well as the possible areas for future research.

2. LITERATURE REVIEW

2.1 Stainless steel

Stainless steel is a group of materials that are iron-based alloys, with a minimum chromium content of 10.5%. This content of chromium is the responsible for its high corrosion resistance, allowing a self-repairing layer of chromium oxide to form, protecting the surface. This layer is activated when exposed to air or any other oxidizing environment, it's transparent and tightly adherent, with a thickness of $5x10^{-6}$ mm (Design Manual for Structural Stainless Steel DMSSS, 2017). This corrosion resistant property makes stainless steel very valuable in highly aggressive and corrosive environments, such as marine environments, chemical industries and wastewater treatment plants but also in the food processing industry mainly because of the requirement of clean surfaces (Becque et al., 2006).

There are other alloying elements as nickel, molybdenum, titanium and copper, which are added in order to enhance some material properties (mechanical and physical), such as increase the stability of the passive layer and also improve ductility and weldability. This allows obtaining a wide range of stainless steel grades suitable for various specific uses because of their varying levels of corrosion resistance and strength (Arrayago, 2016).

According to their atomic structure, stainless steels are categorized into these main groups: austenitic, ferritic, duplex, martensitic and precipitation hardening stainless steel. The selection of the type of stainless steel will depend on the requirements and conditions of the application, mainly to the environment (corrosion conditions), service life, but also depends on the properties of the material as the ability to bear crevice, pitting, abrasion and interganular corrosion. In Figure 1 (DMSSS, 2017) is shown the classification of stainless steels according to their nickel and chromium content.

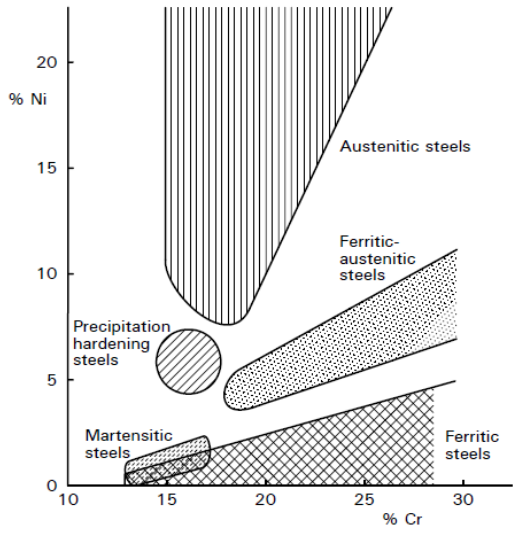

Figure 1. Classification of stainless steel according to nickel and chromium content, DMSSS

2.1.1 Types of stainless steel

Austenitic stainless steel

Austenitic stainless steels are the most frequently used in building and construction, they are usually based on 17% to 18% chromium and 8 to 11% nickel additions, being this nickel content responsible for its high cost. They have a face-centered cubic atomic structure; therefore they happen to have high ductility beside to their corrosion resistance. They also have significantly good toughness over a wide range of temperatures, and can be strengthened by cold-working. (DMSSS, 2017)

This material is generally selected for structural applications, as mentioned before, mainly because of the combination of its good strength, corrosion resistance, and high ductility which is determining for seismic applications.

Ferritic stainless steel

Generally the chromium content of the ferritic stainless steels is between 10.5% and 18% and their nickel content is either very small or zero, therefore their cost is lower and more stable than for the austenitic grades with equivalent corrosion resistance. They have a body-centered atomic structure and they can also be strengthened by cold-working. They also have good resistance to stress corrosion cracking and their corrosion performance can be further enhanced by additions of molybdenum. On the other hand they are generally less ductile and less weldable than austenitic stainless steel. (DMSSS, 2017)

Duplex stainless steel

According to the DMSSS (2017) the duplex alloys consist of a mixed crystal structure of austenitic and ferritic stainless steel. They typically contain 20 to 26% chromium, 1 to 8% nickel, 0.05 to 5% molybdenum and 0.05 to 0.3% nitrogen. As they contain less nickel than austenitic grades the offer less price volatility. They can be twice as strong as austenitic steels in the annealed condition, which can lead to size reduction, very important in weight-sensitive structures (like bridges). They also shiw a good corrosion resistance and hence they are suitable for a broad range of corrosive environments. They can be strengthened by cold-working, have good weldability and good resistance to stress corrosion cracking.

Duplex stainless steel is usually selected when high strength, corrosion resistance and higher levels of crevice and stress corrosion cracking resistance are required.

2.1.2 Material response

Stainless steel has a notorious different stress-strain behavior from carbon steel, especially in the shape of the stress-strain curve, which is dominated by non-linearity (DMSSS, 2017). Carbon steel curve initiates at the elastic region with a clearly defined yield point followed by a yielding plateau whilst stainless steel shows a non-linear stress-strain response even for low strain levels, characterized by its rounded shape with no well-defined yield point strength. The yield point of non-linear materials such as stainless steel

is conventionally determined as the proof stress for a 0.2% offset strain (Arrayago (2016), Afshan et al. (2017)).

The other big difference between these materials is that stainless steels exhibit a considerable strain hardening and high ductility, whence it can absorb considerable impact without fracturing, reaching strains at fracture of 40-60%, for the most ductile austenitic grades. (Arrayago, 2016).

In Figure 2 (DMSSS, 2017) the stress-strain curves for different stainless steels families and carbon steel are shown, where the mentioned non-linearity of the stainless steels can be observed. The figure also shows the different response of ferritic stainless steels, offering more strength than carbon steel but less roundness than austenitic stainless steel.

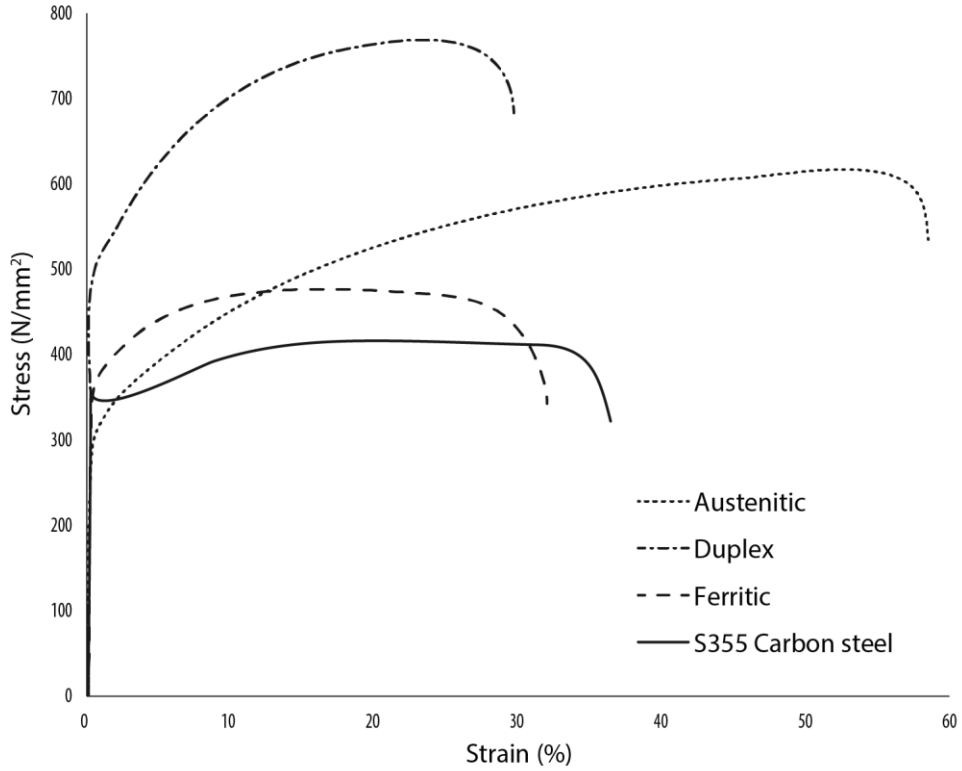

Figure 2. Stress-strain curves for different stainless steels families and carbon steel

There are certain factors that can change the shape of the basic stress-strain curve for any given grade of stainless steel. Cold-working is one of them, during this process the properties of the material are enhanced, whence the price is a little higher than the equivalent annealed material, depending on the grade, product form and level of cold working. Due to this process, stainless steel tends to exhibit non-symmetry of tensile and compressive behavior and anisotropy, which consists in different characteristics presented in parallel and transverse to the rolling directions. The thinner sections (thickness below 3mm) are the most affected by cold-working (DMSSS, 2017).

As plastic deformations occur during the fabrication of a section by cold-forming, there is a significant increase in the 0.2% proof strength. Usually this strength enhancement is of about 50%, and is presented in the cross-section corners, although the material in the flat faces also increases (DMSSS, 2017).

2.1.3 Material models

In order to better comprehend the non-linear stress-strain behavior of stainless steel and enhance the knowledge about the material to provide a more safe, accurate and economic design, it is necessary to develop several material models to describe analytically the stress-strain curve.

The most widely used material modes are based on the general expression originally proposed by Ramberg and Osgood (1943), and have been developed in the last decades. The Ramberg and Osgood expression was modified by Hill (1944) as given in Eq. (1), where E is the Young's modulus, $\sigma_{0.2}$ is the 0.2% proof stress conventionally considered as the yield stress, and n is the strain hardening exponent which characterizes the roundness of the stress-strain curve (Arrayago et al., 2015).

The basic Ramberg-Osgood formulation is able to accurately representing different regions of the stress-strain curve, depending on the n parameter chosen, but has been shown to be generally incapable of accurately representing the full stress-strain curve with a single value of n. For this reason there have been other two-stage Ramberg-Osgood models that have been developed to provide a single continuous representation of the stress-strain curve of stainless steel. Mirambell and Real (2000) proposed a two-stage model based on the Ramberg-Osgood expression, but defining a second curve for stresses above the $\sigma_{0.2}$ proof stress given in Eq. (2), with an additional strain hardening exponent m for the second stage. In this equation $E_{0.2}$ is the tangent modulus at the 0.2% proof stress, σ_u and ε_u are the ultimate strength and strain and $\varepsilon_{0.2}$ is the total strain at the 0.2% proof stress (Arrayago et al., 2015). These values can be obtained experimentally or by calculation, using the correspondent expressions.

$$\varepsilon = \frac{\sigma}{E} + 0.002\left(\frac{\sigma}{\sigma_{0.2}}\right)^n \quad for\ \sigma \leq \sigma_{0.2} \tag{1}$$

$$\varepsilon = \frac{\sigma - \sigma_{0.2}}{E_{0.2}} + \left(\varepsilon_u - \varepsilon_{0.2} - \frac{\sigma_u - \sigma_{0.2}}{E_{0.2}}\right) * \left(\frac{\sigma - \sigma_{0.2}}{\sigma_u - \sigma_{0.2}}\right)^m + \varepsilon_{0.2} \quad for\ \sigma \geq \sigma_{0.2} \tag{2}$$

This model proposed by Mirambell and Real was later simplified by Rasmussen (2003), with the purpose of reduce the required input parameters, leading to the revised expression for $\sigma > \sigma_{0.2}$ .Rasmussen (2003) also developed expressions to determinate the second strain hardening parameter m, the ultimate strain and strength (ε_u and σ_u, respectively), effectively reducing the number of required input parameters to three basic Ramberg-Osgood parameters (E, $\sigma_{0.2}$ and n). This proposal was included in EN 1993-1-4,

Annex C (2006) for the modeling of stainless steel material behavior (Arrayago et al., 2015), and is shown in Eq. (3).

$$\varepsilon = 0.002 + \frac{f_y}{E} + \frac{\sigma - \sigma_{0.2}}{E_y} + \varepsilon_u * \left(\frac{\sigma - f_y}{f_u - f_y}\right)^m \quad for\ \sigma_{0.2} < \sigma \leq \sigma_u \tag{3}$$

The Mirambell and Real model was also modified by Gardner and Ashraf (2006) in order to improve the accuracy of the model at low strain and also allow the model to be applied for the description of compressive stress-strain behavior. A further two-stage model was also proposed by Gardner et al. (2010) to stainless steel material modeling in fire.

There are some situations that require an accurate material description up to very high strains, for example the need to represent cold-forming processes and connection behavior. This requirement led to the development of three-stage versions of the Ramberg-Osgood formulation by Quach et al. (2008) proposing a material model using basic Ramberg-Osgood curve for the first stage, covering stresses up to the 0.2% proof stress, the Gardner and Ashraf model (2006) to cover stresses up to 2% proof stress for the second stage and a straight line from the 2% proof stress to the ultimate strength for the third stage. More recently, Hradil et al. (2013) proposed an alternative three-stage model but using the Ramberg-Osgood equation for every stage, using different reference systems in each stage.

2.1.4 Life cycle cost and environmental impact

One of the most important issues when choosing materials in the design stage must be life cycle costs and not just initial costs as usually occurs. According to the Design Manual for Structural Stainless Steel (2017) selecting a corrosion resistant material in construction industry is very determining, as future maintenance could be avoided (or reduced), costs associated to replacement and downtime can also be reduced, although initial costs are usually higher.

This is the case for structural stainless steel, whose initial cost is considerably higher than for an equivalent carbon steel product, although there can be initial cost savings associated with eliminating corrosion resistant coatings. Also when high strength stainless steel is used, material requirements can be reduced because of the decreasing section size and overall structure weight, reducing initial costs. Furthermore the need for coating maintenance is eliminated as is the component replacement due to corrosion, reducing widely long-term maintenance costs. Another advantage to consider is the reduced inspection frequency and costs associated with stainless steel due to its excellent corrosion resistance, and long service life (DMSSS, 2017).

The environmental impact of the materials should also be determined when designing. According to this principle stainless steel is once more a good option because of its high value at the end of the structure life (scrap value). Due to this high residual value, scrap is recycled into new metal and end-of-life recycling rates are very high, although for the

moment the scrap availability is limited due to the material's high service life (DMSSS, 2017).

All types of stainless steel have a typical recycled content of at least 60%, since stainless steel is 100% recyclable and can be indefinitely recycled into new high quality stainless steel (DMSSS, 2017).

2.1.5 Structural use

Stainless steel has been used in construction since it was created, around 1910, but its use is increasing considerably during last decades. This increasing use of stainless steel in the construction industry is due to its great properties such as high corrosion and fire resistance, aesthetic appeal, good strength, toughness and fatigue properties. These aspects in addition to reduced maintenance costs and requirements as low lifecycle costs can compensate the high unit price of stainless steel, in comparison to carbon steel (Becque et al., 2006).

Another important property of this material is its high ductility, which is a determining factor if resistance to seismic actions is required, that is to say in seismic zones.

Austenitic and duplex grades common applications in the construction industry are: beams, column and platforms in water treatment plants, chemical, food, and nuclear industries among others, in bridges, security barriers, hand railing, structural members and fasteners in swimming pool buildings, explosion-and impact- resistant structures, fire and explosion walls, cable ladders and walkways on offshore platforms, etc. (DMSSS, 2017)

Ferritic grades are used in the transportation sector, for load-bearing members. Although they are not commonly used for structural members, they have the potential of being used for strong and durable structural elements with attractive metallic surface. This greater application is also combined with the possibility of their use in composite structures, where a long service life is mandatory, or if the environment is corrosive, since ferritic grades may provide a more economically viable solution than other materials (such as galvanized steel for example). (DMSSS, 2017)

Design rules codified for carbon steel cannot directly be applied to stainless steel structural members, because of the considerable differences between these materials and, therefore numerical and theoretical research is needed to develop pertinent design rules and ensure a safe and accurate design for stainless steel structures.

There are many recent examples of stainless steel structures, combining notorious aesthetical appearance with good structural behavior. One example of this is the Helix Bridge, a pedestrian bridge located in the Marina Bay area in Singapore (see Figure 3), opened in 2010. It's made of duplex steel (EN1.4462), and its shape represents the geometric helicoidal arrangement of DNA by using two helix structures that act as a truss to resist the design loads. This bridge is 280 m long, with three spans of 65 m and two end spans of 45 m. The tropical climate of the location, and the marine environment were key

to the selection of the bridge's material, which needed to be highly corrosion resistant. The abutments of the bridge are made of concrete.

Figure 3. Helix Bridge in Singapore (Image by Arch Daily)

2.1.5.1 Use of cold-formed

Thin-walled cold-formed sections are widely used because they offer an interesting field of applications for stainless steel. The first reason is stainless steel is widely available in thin sheets, because its extensive use in various non-structural applications. Another reason is that thanks to the cold-working during the manufacturing process the strength levels of corner areas get enhanced, therefore improving the response of members. And finally the use of stainless steel eliminates the natural vulnerability to corrosion of carbon steel thin-walled sections due to their large surface to volume ratio. (Becque et al., 2006).

2.1.6 International design standards

The "Specification for the Design of Light Gauge Cold-Formed Stainless Steel Structural Members" was the first standard for the design of structural stainless steel, published in 1968 by the American Iron and Steel Institute (AISI) and was based on the work by Johnson and Winter (1966). In 2002, after some revisions by the American Society of Civil Engineers (ASCE) and the AISI, was published the latest American specification for

structural stainless steel “Specification for the Design of Cold-Formed Stainless Steel Structural Members” SEI/ASCE 8-02 (2002).

The first European design guide for structural stainless steel was the “Design Manual for Structural Stainless Steel”, published in 1994 by EuroInox. Later in 1996 the European Standards Committee CEN released the European pre-standard for stainless steel, “EN 1993-1-4: Design of Steel Structures-Supplementary rules for stainless steel”, and was based from the first Design Manual. This pre-standard was later converted to the current European standard EN1993-1-4 (2006). The fourth edition of the “Design Manual for Structural Stainless Steel” and its commentary has been published by the Steel Construction Institute in collaboration with several European universities and research centers in the frame of a RFCS research project (2017).

The Australian/New Zealand stainless steel design standard was published in 2001, and called “AS/NZS4673: 2001 Cold-Formed Stainless Steel Structures”. It was published by the Joint Technical Committee and was based on the American Specification.

2.2 Stainless steel open sections

Theoretical work on inelastic buckling of plates was developed by Bleich (1952), based on the work of Stowell (1948). Furthermore, Johnson and Winter (1966) conducted experimental work on cold-formed stainless steel hat sections, proposing the expressions to calculate the effective width of the class 4 sections, and concluded that the standard Winter equations valid for carbon steel where able to be applied to stainless steel cold-formed sections.

Further experimental and theoretical work was developed by Rasmussen, Burns et al. (2004) about the local buckling of both single stainless steel plates and cold-formed stainless steel sections, demonstrating that the effect of gradual yielding in cold-formed section is offset by the enhanced corner properties. Therefore both the American and the Australian design codes for stainless steel are based on the classical Winter equations to calculate effective widths.

The objective of this work is to gain knowledge about the behavior of open sections, angle sections specifically, when subjected to pure compression and extend the numerical research in this matter.

2.2.1 Angle sections

Angle sections have been extensively used in various applications because of different reasons, one of them is their wide range of different sizes available (Kettler, 2016).

According to Kettler (2016) and Jain (2014) angle sections are used in structural applications especially in members with primary axial forces, because of their relatively simple connections and the simplicity of their fabrication process. Other advantages for the construction industry of this particular section are its compactness, lightness in weight and economic transportation. However its structural behavior is quite complex, mainly because

its centroid lies outside the section hindering the application of the forces.Therefore, steel angle columns show generally two main failure modes, torsional-flexural and flexural buckling.

This complex structural response has been studied for years by different researchers and engineers, developing different models and tests, which are exposed in this chapter.

In carbon steel there are many works about the design of steel angles contrasting to stainless steel where the available information is considerably reduced. Popovic et al. (1999) presented their work on fix-ended and pin-ended compression tests of cold-formed angles, comparing their results with the Australian and American specifications. There were a series of papers published by Trahair in 2002 and 2005, about the behavior and design of single angle sections and where formulation to predict the lateral buckling strength of steel angles was proposed. Later, Young (2004) discussed Trahair's work and presented himself a series of tests on the design of angle columns. Also Rasmussen (2005) studied steel angle columns with locally unstable legs, and then extended it to the design of steel angle beam-columns and the use of the Direct Strength Method (DSM). More recently Li (2012) compared different design methods to determine the axial capacity of hot-rolled equal-leg single angles, showing that the axial compressive strength for the same angle and same unbraced length varies considerably with the different design methods. In 2014 Jain et al. studied the lateral-torsional buckling of laterally unsupported single angle sections loaded along geometrical axis, comparing their results with the existing provisions of AISC specification, and also aiming to develop design relations for the Indian steel design code IS 800:2007 (Jain et al., 2014). Dinis et al. presented in 2015 their experimental work developing a new design approach for fixed-ended and pin-ended columns, based on the Direct Strength Method. A specific single angle design method was incorporated into the Specification for Structural Steel Buildings (AISC) in 2005 as a result of some of these studies.

The section to study in this work corresponds to an equal-leg single angle as it's shown in Figure 4.

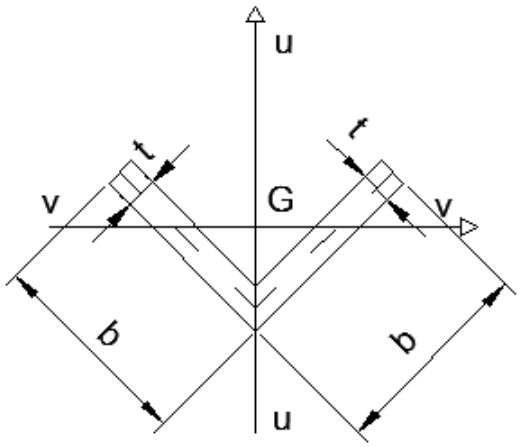

Figure 4. Equal-leg single angle cross-section

For the design of the member, it is necessary to determine its ultimate capacity, whether is the cross-section response or the member response, in order to safely design the element. According to the Eurocode this is achieved through the Ultimate Limit State Method which exposes that when one of these states is exceeded it can lead to collapse of parte or the whole of the structure, whence the following expression needs to be satisfied:

$$E_d \leq R_d \tag{4}$$

Where:

E_d is the design value of the effect of actions such as an internal moment or vector in the member or element under consideration due to the factored applied loading acting on the structure.

R_d is the resistance of the structure.

2.2.3 Cross-section response

2.2.3.1 Formulation for cross-sectional resistance

As said before, it is necessary to determine the ultimate capacity of the cross-section in order to safely design a structure, verifying if the section is capable of resisting all the forces it is subjected to. Instabilities also need to be taken into account, since they can be often limiting.

As exposed in the European design standard Eurocode 3 Part 1-1 (2005) the first issue to define is the cross-section class. This classification depends on the susceptibility to local buckling and the rotation capacity of the section. According to the European design standard Eurocode 3 Part 1-4 (2006) the classification of stainless steel angle sections consists in:

- Class 3: cross-sections are those in which the calculated stress in the extreme compression fiber of the steel member can reach its yield strength, but local buckling appears before it reaches its plastic moment resistance.
- Class 4: local buckling occurs before the section reaches yield strength.

The limits to classify the cross-section for angles according to the EN1993-1-4+A1:2015 are shown in Figure 5. These limits are the same for the DMSSS (2017).

Angles

Refer also to "Outstand flanges" (see sheet 2 of 3)

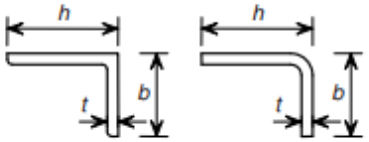

Does not apply to angles in continuous contact with other components

Class	Section in compression
Stress distribution across section (compression positive)	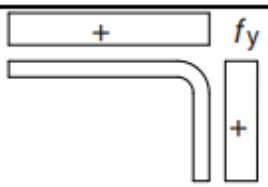
3	$h/t \le 15\varepsilon$: $\frac{b+h}{2t} \le 11{,}5\varepsilon$

$$\varepsilon = \left[\frac{235}{f_y}\frac{E}{210\,000}\right]^{0,5}$$

Grade	1.4301	1.4401	1.4462
f_y (N/mm^2)	210	220	460
ε	1,03	1,01	0,698

Figure 5. Limits to classify the cross-section for angles according to the EN1993-1-4+A1:2015

When the cross-section is Class 4 section it is necessary to reduced it, since not all of it is effective. The effective area of a Class 4 cross-section, A_{eff} is the gross area of the cross-section minus the sum of the ineffective areas of each member of the cross-section. In order to calculate this effective area, the effective breadth b_{eff} needs to be determined, and then multiplied by the member thickness.

The reduction factor ρ needs to be calculated to determine the effective breadth, as follows in Eq. (5) and Eq. (6) according to EN1993-1-4+A1:2015:

$$\rho = \frac{1}{\overline{\lambda_p}} - \frac{0.188}{\overline{\lambda_p}^2} \le 1 \tag{5}$$

$$\overline{\lambda_p} = \frac{\bar{b}/t}{28.4 * \varepsilon * \sqrt{k_\sigma}} \tag{6}$$

The expression (5) is for outstand elements, and there is another one for internal elements.

Where:

$\overline{\lambda_p}$ is the element slenderness

$\bar{b}$ is the relevant width (h for equal leg angles)

t is the relevant thickness

ε is the material factor defined in Figure 5

k_σ is the buckling factor corresponding to the stress ratio ψ and boundary conditions.

The resistance of a cross-section subjected to compression $N_{c,Rd}$ with a resultant acting through the centroid of the gross section (or the effective section for Class 4 cross-sections), may be calculated as shown in Eq (7).

$$N_{c,Rd} = \frac{A * \sigma_{0.2}}{\gamma_{M0}} \quad (7)$$

Where:

A is the cross-sectional area

$\sigma_{0.2}$ is the characteristic yield strength (generally taken as the minimum specified 0.2% proof strength).

Υ_{M0} is the partial factor for cross-sections.

2.2.4 Member response in compression

Early work on inelastic column buckling was established by Engesser (1889) and Shanley (1947). Jhonson and Winter (1966) also conducted various tests on stainless steel channels (columns) arranged in both closed box and I-section configurations and confirmed the validity of the tangent modulus approach. Since then various studies have been conducted on the overall buckling capacity of stainless steel considering with different types of cross-section.

2.2.4.1 Previous experimental programmes on angle section members

Angle sections present a highly complicated structural behavior as mentioned before, and have not been studied as much as other open sections of carbon steel, furthermore the experimental programmes on stainless steel angle sections are even less common and experimental data is considerably limited. Consequently the design standards of stainless steel are very conservative, which leads to the oversizing of the members.

The lack of stainless steel angle experimental data is observed in Table 1, where the available flexural buckling tests are presented.

Table 1. Previous experimental programmes on angle sections

Steel	Grades	Reference	No. of tests/ FE Models
Carbon steel	-	Young and Chen, 2008	25
Carbon steel	-	Schifferaw and Schafer, 2014	88
Carbon steel	-	Kettler et al., 2016	126
Carbon steel	-	Landesmann et al., 2016	77
Carbon steel	-	Maia et al., 2016	78
Carbon steel	-	Jain and Rai, 2014	24
Carbon steel	-	Popovic et al.	30
Stainless steel	Austenitic 1.4301	De Menezes et al., 2017	11
Stainless steel	Austenitic 1.4301	Dobric	59

2.2.4.2 Formulation for member resistance

Flexural and torsional-flexural buckling are the two main failure modes for angles, and therefore it is necessary to check the members for these buckling modes. This section presents the prescriptions codified in EN 1993-1-4 (2006) and DMSSS (2017) for flexural buckling and torsional-flexural buckling.

2.2.4.3 Flexural buckling

The flexural buckling resistance of members $N_{b,Rd}$ can be calculated as follows in Eqs. (8), (9) and (10), according to EN 1993-1-4 (2006) and DMSSS (2017). These expressions are based on the Perry-Robertson formulation established in EN1993-1-1 (2005) for carbon steel members, therefore the particular behavior of stainless steel is taken into account by considering different buckling curves and limiting slenderness.

$$N_{b,Rd} = \chi * \frac{A * \sigma_{0.2}}{\gamma_{M1}} \tag{8}$$

$$\chi = \frac{1}{\varphi + \left[\varphi^2 - \bar{\lambda}^2\right]^{0.5}} \leq 1 \tag{9}$$

$$\varphi = 0.5 * (1 + \alpha * \left(\bar{\lambda} - \bar{\lambda}_0\right) + \bar{\lambda}^2) \tag{10}$$

Where:

χ is the reduction factor due to flexural buckling.

A is the cross-sectional area (For cross-section Class 4 the effective area (A_{eff}) needs to be adopted)

γ_{M1} is the instability partial safety factor.

α is the imperfection factor depending on the type of member (cross-section type and fabrication process)

$\bar{\lambda}_0$ is the limiting non-dimensional slenderness depending on the type of member

For flexural buckling the Eurocode EN 1993-1-4 (2006) considers less conservative buckling curves than those proposed in the Design Manual for Stainless Steel (2017), because at the time the experimental data was considerably limited. Over the last ten years it has been demonstrated that the EN 1993-1-4 (2006) buckling curves for tubular sections are excessively optimistic, and it is expected that the next revision to this code will give the flexural buckling curves proposed in the DMSSS (2017). In the Tables 2 and 3 the values for buckling curves in EN 1993-1-4 (2006) and in DMSSS (2017) are shown, respectively.

Table 2. Values for flexural buckling in EN 1993-1-4 (2006)

Type of member	**Axis of buckling**	**α**	$\bar{\lambda}_0$
Cold-formed open sections	Any	0.49	0.40
Hollow sections (welded and seamless)	Any	0.49	0.40
Welded open sections	Major	0.49	0.20
	Minor	0.76	0.20

Table 3. Values for flexural buckling in DMSSS (2017)

Type of member	**Axis of buckling**	**Austenitic and duplex**		**Ferritic**	
		α	$\bar{\lambda}_0$	**α**	$\bar{\lambda}_0$
Cold-formed open angles and channels	Any	0.76	0.2	0.76	0.2
Cold-formed lipped channels	Any	0.49	0.2	0.49	0.2
Cold-formed RHS	Any	0.49	0.3	0.49	0.2
Cold-formed CHS/EHS	Any	0.49	0.2	0.49	0.2
Hot finished RHS	Any	0.49	0.2	0.34	0.2
Hot finished CHS/EHS	Any	0.49	0.2	0.34	0.2
Welded or hot rolled open sections	Major	0.49	0.2	0.49	0.2
	Minor	0.76	0.2	0.76	0.2

In Figure 6 the buckling curves proposed in the DMSSS are shown.

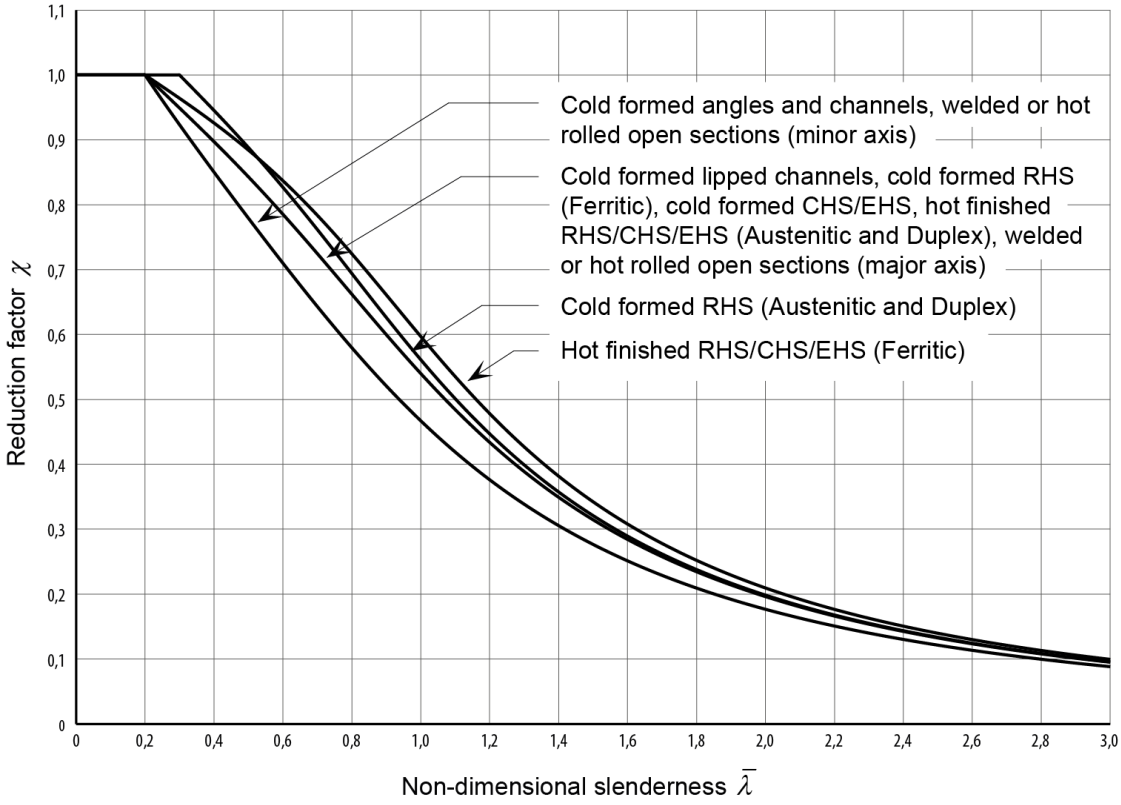

Figure 6. Buckling curves proposed in the DMSSS (2017)

Regarding stainless steel angle sections rotating along their minor axis, DMSSS provides that the buckling curve d needs to be considered.

2.2.4.4 Torsional and torsional-flexural buckling

The resistance of a member to these buckling modes should be determined as follows in Eqs. (11), (12), (13), (14) and (15). According to EN1993-1-4 (2006) and DMSSS (2017) the buckling curve defined through α=0.34 and $\bar{\lambda}_0$=0.2 parameters needs to be considered.

$$\overline{\lambda_T} = \sqrt{\frac{A * \sigma_{0.2}}{N_{cr,T}}} \tag{11}$$

$$N_{cr,T} = \frac{1}{i_o^2} * (G * I_t + \frac{\pi^2 * E * I_w}{l_t^2}) \tag{12}$$

$$i_o^2 = i_y^2 + i_z^2 + y_o^2 + z_o^2 \tag{13}$$

$$N_{cr,TF} = \frac{N_{cr,y}}{2\beta}\left[1 + \frac{N_{cr,T}}{N_{cr,y}} - \sqrt{\left(1 - \frac{N_{cr,T}}{N_{cr,y}}\right)^2 + 4\left(\frac{y_o}{i_o}\right)^2 \left(\frac{N_{cr,T}}{N_{cr,y}}\right)}\right] \quad (14)$$

$$\beta = 1 - \left(\frac{y_o}{i_o}\right)^2 \quad (15)$$

Where:

$N_{cr,T}$ is the elastic critical torsional buckling force.

$N_{cr,TF}$ is the elastic critical torsional-flexural buckling force.

i_y and i_z are the radii of gyration of the gross cross-section about the y and the z axes respectively

y_o and z_o are the shear center co-ordinates with respect to the centroid of the gross cross-section

G is the shear modulus

l_t is the buckling length of the member for torsional buckling

I_t is the torsional constant of the gross cross-section

I_w is the warping constant of the gross cross-section

$N_{cr,y}$ and $N_{cr,z}$ are the elastic critical axial force for flexural buckling about the y-y and z-z axes respectively. The y and z axes should be taken as the u and v axes respectively.

For angle sections the torsional and warping constant are calculated as given in Eqs. (16) and (17) respectively, according to the Spanish Steel Design Code (EAE):

$$I_t = \frac{2}{3} b * e^3 \quad (16)$$

$$I_w = \frac{A^3}{144} \quad (17)$$

Where:

b is the width (h for equal leg angles)

e is the thickness

A is the cross-sectional area

3. NUMERICAL ANALYSIS: FINITE ELEMENT MODELS

3.1 Introduction

In this chapter the numerical analysis is described, exposing the relevant information regarding the Finite Element (FE) analysis conducted in this thesis. The models were made using the general-purpose package ABAQUS. First, the numerical models were developed to replicate experimental tests on angle sections subjected to compression from the literature in order to validate the model. These analyses are shown in section 3.3. After the FE models were validated, a parametric study had been conducted to study stainless steel angle sections subjected to compression, to generate supplementary information on this structural behavior due to the lack of experimental data, especially in stainless steel. General assumptions are first presented in this section, followed by the comparison of the numerical and (existing) experimental results, validating the model. And finally the parametric study is presented.

3.2 General assumptions

The Finite Element (FE) models were conducted by the general-purpose software ABAQUS, in order to correctly represent the structural behavior of angle sections, due to the lack of information and experimental data.

These general assumptions apply for the validation of the model as for the parametric study. The specific characteristics for each case of imperfection amplitudes, dimensions and material are exposed in each section.

For both cases (validation and parametric study) first a linear buckle analysis (Eigenvalue analysis) was carried out, in order to obtain the deformed buckle shape of the member, to finally add it has an initial geometric imperfection in the non-linear analysis.

The general assumptions and characteristics defined in the models are presented next.

3.2.1 Model

It is necessary to create a model that represents the geometry of the studied element, along with the material properties and the boundary conditions.

a) First, defining the geometry of the section was necessary; this was made by creating a Part, selecting a shell shape, type extrusion. This allows to easily draw the shape of the cross-section, and then extrude the section with the corresponding length.
b) Secondly, the material needs to be defined, by introducing its elastic and plastic behavior. This is achieved by entering the following parameters: Young's Modulus (E), and Poisson's Ratio (considered as 0.3 for all models). For the plastic behavior the values of the actual stress-strain curve need to be added. Abaqus requires this information in form of true stress (σ_{true}) and true log plastic strain (ε_{true}), these are

obtained from the engineering stress-strain curves ($\sigma_{nom} - \varepsilon_{nom}$), given in Eqs. (18) and (19).

$$\sigma_{true} = \sigma_{nom}(1 + \varepsilon_{nom}) \tag{18}$$

$$\varepsilon_{true} = \ln(1 + \varepsilon_{nom}) - \frac{\sigma_{true}}{E} \tag{19}$$

c) After this a section was defined, where the shell thickness is introduced and the material of the section is specified. This section is assigned to the created Part.
d) In the Interaction module the Constraints are created using the Coupling type. In all the models there are two control or reference points, located at the ends of the member, therefore there are two constraints. For this, it's necessary to select the constraint control points (RP1 and RP2, which need to be created before), select "surface" as the constraint region point and finally select this corresponding surface. Then, it was necessary to define the coupling type which was Kinematic and to constrain all degrees of freedom, meaning that all the surface's displacements and rotations will be limited by the reference point. The axial load was applied through one of these reference points, while the longitudinal displacement of the other reference point constrained.

3.2.2 Steps

To define the analyses and their particular conditions (boundary conditions, external actions, etc.) different steps need to be defined. This is done in the Step module, where an Initial step is created. Each Step contains one analysis. First a linear buckling analysis is necessary to obtain the buckling mode deformed shape of the member, and then, as mentioned before, add this deformed shape as an initial geometric imperfection in a non-linear analysis.

a) The buckle analysis is defined from the procedure type "Linear perturbation", and a number of 12 eigenvalue were requested. For this step the boundary conditions are: the displacements of one end of the column are zero and on the other end of the column there is a predefined displacement along the longitudinal axis of the member, and compressing the member. All other displacements are restrained. The rotations of both of the ends depend on whether it's pin-ended or fix-ended, this was determined according to each case (validation of the model and the parametric study).
b) The final step is created to carry out the non-linear analysis, therefore the Static, Riks analysis was chosen. This is a non-linear analysis that allows to find static equilibrium states during the unstable phase of the response using Newton's method, and is widely used for cases where the loading is proportional (ABAQUS, 2012). In this step it is necessary to include the geometrical non-linear effects of large displacements or second order effects, by indicating Nlgeom "On". Also it is very important to define the increase type of the analysis. In this case the option

"Automatic" was set, allowing ABAQUS to choose the arc length increment sizes based on computational efficiency. Later, the arc length increment values need to be specified, (Initial, Minimum, Maximum and Estimated total arc length) to obtain the expected results. Defining the specific boundary conditions for this step is now necessary, and they coincide with those in the Buckle step, the displacements of one end of the column are zero, on the other end of the column there is a predefined displacement, representing the axial load, along the longitudinal axis of the member, and compressing the member. All other displacements are restrained. The rotations of both of the ends depend on whether it's pin-ended or fix-ended condition.

For both analyses the imposed displacements values vary from 2mm to 6mm, according to each configuration.

3.2.3 Mesh

Before analyzing the model it is necessary to create the mesh, in order to divide the member into smaller elements to correctly replicate its real behavior.

The mid-surfaces of the cross-sections were modeled by using the four-node shell elements with reduced integration S4R. This element (S4R) is a robust, general-purpose element that is suitable for a wide range of applications, providing accurate solutions in all loading conditions for thin and thick shell problems (ABAQUS, 2012). It uses uniformly reduced integration to avoid shear and membrane locking, and do not have any unconstrained hourglass modes.

After conducting a mesh convergence study the size of the mesh was 5mm x 5mm, in both types of analysis, in order to obtain accurate results with a reasonable computational effort (Lendesmann et al. (2017), Arrayago (2016)).

3.2.4 Residual stress

Residual stresses were not taking into account in the analyses, since it has been reported in the literature that the influence of residual stresses is negligible on the angle column failure loads (Lendesmann et al. (2017), Jandera and Zhang (2017), Young and Ellobody (2005)).

3.2.5 Initial geometric imperfections

The effect of the initial geometric imperfections in angle sections is very important as for every other section, and needs to be taken into account for every analysis. As mentioned before, its centroid is located outside the section, which difficult the application of the forces. Subsequently initial imperfections could contribute to this uneven behavior of the section, affecting considerably the column capacity. As stated before, an imperfection pattern according to the first buckling mode shape is usually considered in numerical simulations (Beque et al. (2008), Jain and Rai (2014), Kettler et al. (2017)). This shape is determined after conducting an elastic eigenvalue or lineal buckling analysis, before the

non-linear analysis is carried out. This buckle analysis is performed with exactly the same mesh employed in the non-linear analysis, in order to use the deformed shape as the initial geometry of the member. The amplitudes of the equivalent imperfections were taken from the literature, and specified in each case. For short specimens the relevant initial imperfections are the local ones, since cross-section failure is expected unlike for long specimens both global and local imperfections need to be taken into account (Arrayago, 2016).

After the buckling analysis is carried out, the file with extension *.fil is created, which contains the coordinates of the obtained eigenmodes. This is the file that is used as input for the *IMPERFECTION command in the simulation. This command allows combining different eigenmodes as a linear combination if desired, to be used as an initial imperfection.

According to Becque and Rasmussen (2008) depending on the thickness of the member, it is possible that one of the two buckling modes would not appear. If the global buckling mode is not encountered within a reasonable number of requested eigenmodes the shell thickness needs to be sufficiently increased to enforce overall buckling as the primary eigenmode of the member as an alternative to increase the requested number of eigenmodes. On the contrary if the local mode is not present, the shell thickness can be reduced sufficiently to ensure a purely local primary eigenmode, with no interference of overall buckling modes. A general view of overall and local buckling modes to be introduced as initial imperfections are shown in Figure 7.

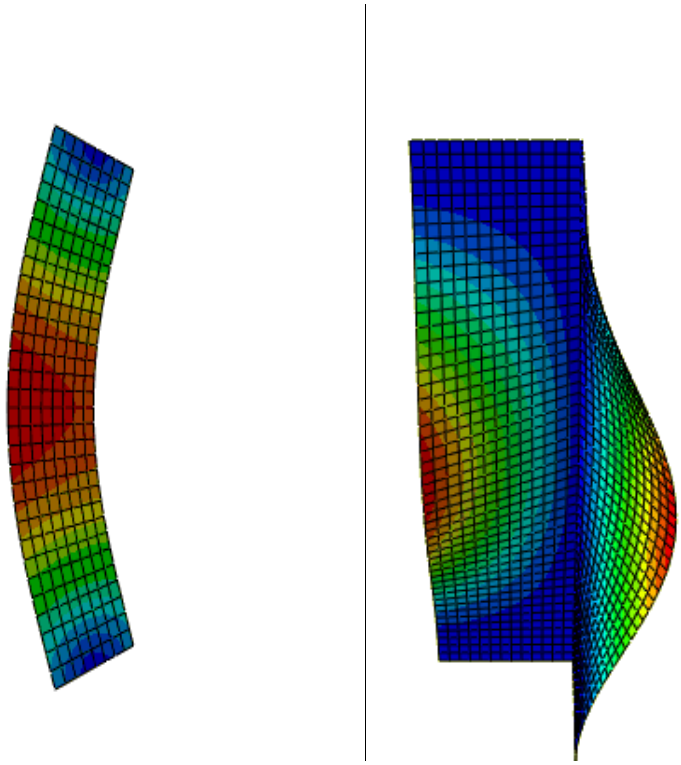

Figure 7. Overall and Local buckling mode

3.3 Validation of the numerical models

The accuracy of the models is investigated by comparing the experimental ultimate loads and the failure mode shapes to those predicted by the FE models. This was made for two different experimental programmes reported by Lendesmann et al. (2017) and by Menezes et al. (2017).

For this, it was necessary to consider the same elements dimensions and different amplitudes of the initial imperfections, in order to correctly adjust the model. Also, the actual material properties were used.

When modeling both models the end points of the columns were kinematically coupled and connected to two reference points, as explained in the previous section, where the degrees of freedom were defined. These reference points were located according to the experiment set-up.

In addition, to simulate the compression force applied in the columns a displacement was fixed along the longitudinal axis of the member.

3.3.1 de Menezes et al. Validation model (2017)

1. Cross-Section:

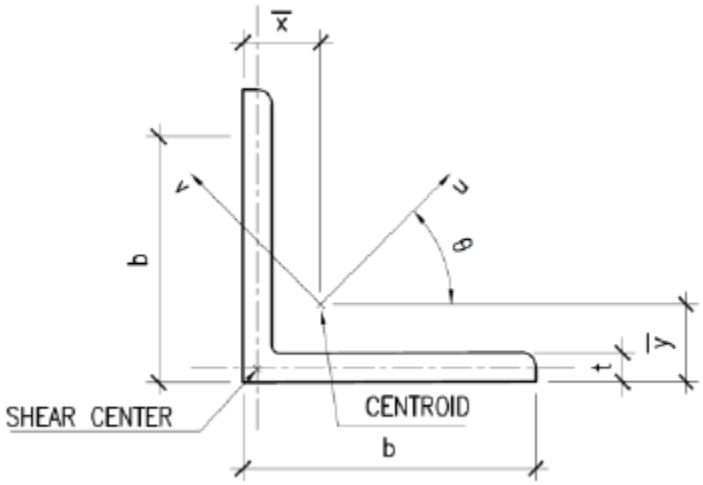

Figure 8. Studied cross-section (de Menezes et al. 2017)

Dimensions: 64x64x6.35 (mm)
Studied Lengths: 500, 1500 (mm)

2. Test configuration: the columns were tested under pure compression to determine the capacity of the angle section member. The column was placed between fixed conditions as specified in the experimental setup (see Figure 9), therefore no rotation was allowed at column ends.

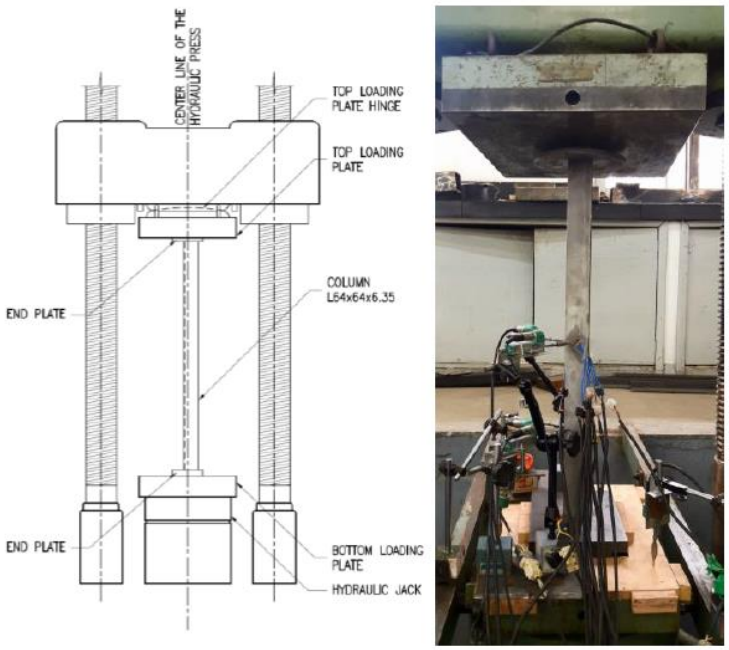

Figure 9. Experimental setup (de Menezes et al. 2017)

The two reference points (RP1 and RP2) were placed at the ends of the column as shown in Figure 10.

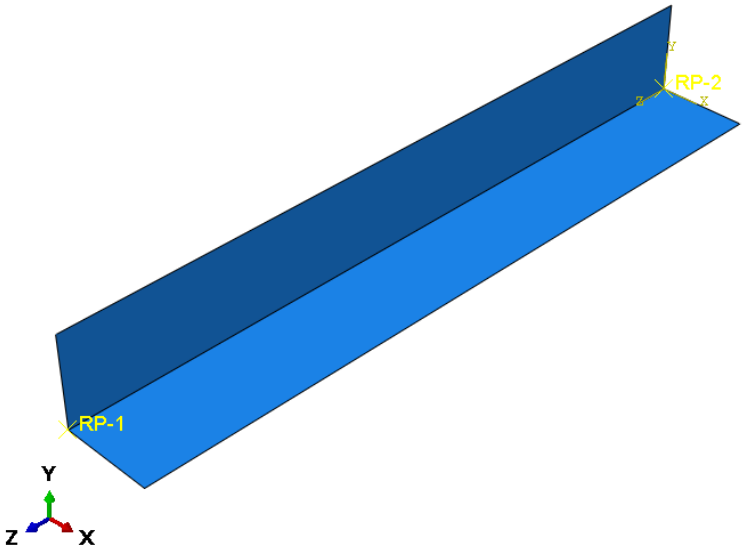

Figure 10. FE model

The border conditions of the model consisted in restraining all movements and rotations as the test configuration shows (see Figure 11). As mentioned before, a displacement of 2mm at the top of the column was applied to simulate the applied force in the member.

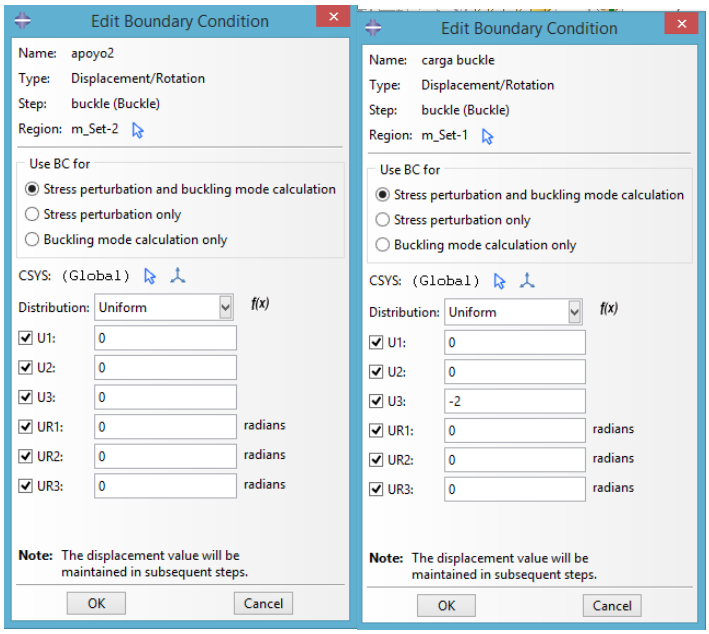

Figure 11. Border conditions applied in the FE model

3. Material

Several material characterization tests were made by the authors, obtaining E=189.2 GPa and $\sigma_{0.2}$=335 MPa. The value of the tensile strength and the corresponding strain are also given, σ_u=713 MPa, ε_u=45%. The other parameters were calculated. With these parameters the stress-strain curve was obtained, shown in Figure 12, using the analytic model exposed in the Model paragraph was used.

The value of the parameter n was chosen to be 3.5, in Table 4 are shown all the parameters and in Figure 12 the resulting stress-strain curve of the material is shown.

Table 4. Material parameters for the FE model validation

AUSTENITIC	
E (MPa)	189200
$\sigma_{0,2}$ (MPa)	335
n	3.5
$E_{0.2}$ (MPa)	38195.73
σ_u (MPa)	713
ε_u	0.45
m	2.315568

Where E is the Young's modulus, $\sigma_{0,2}$ is the 0.2% proof stress (yield stress), $E_{0.2}$ is the tangent modulus at the 0.2% proof stress, σ_u is the ultimate strength and ε_u is the ultimate strain.

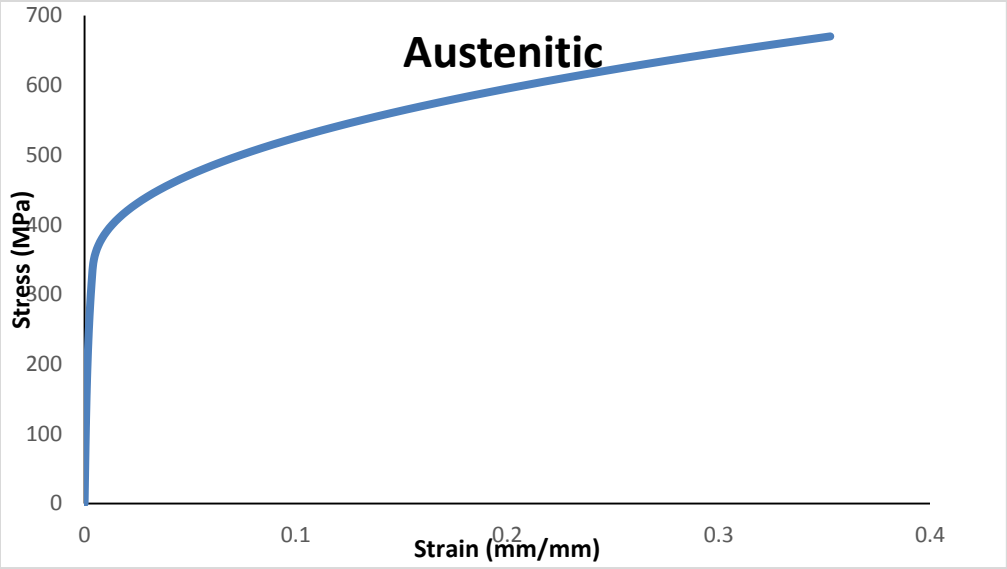

Figure 12. Stress-strain curve of the material

4. Imperfections: a linear buckle analysis was made to determine the buckling modes and eigenvalues.
   The first buckle analysis was made with the original thickness (t=6.35mm), and a local mode was shown for the two member lengths considered, as shown in Figures 13 and 14.

   - L=500 mm

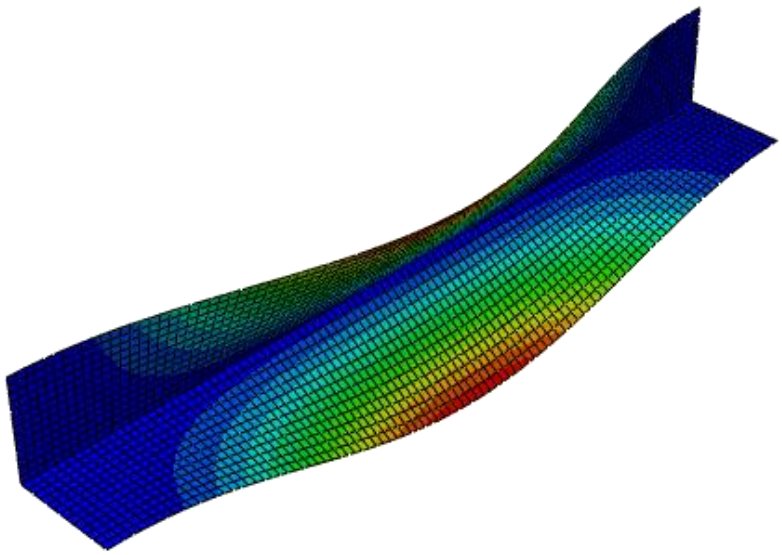

Figure 13. Local failure mode, L=500 mm

- L=1500 mm

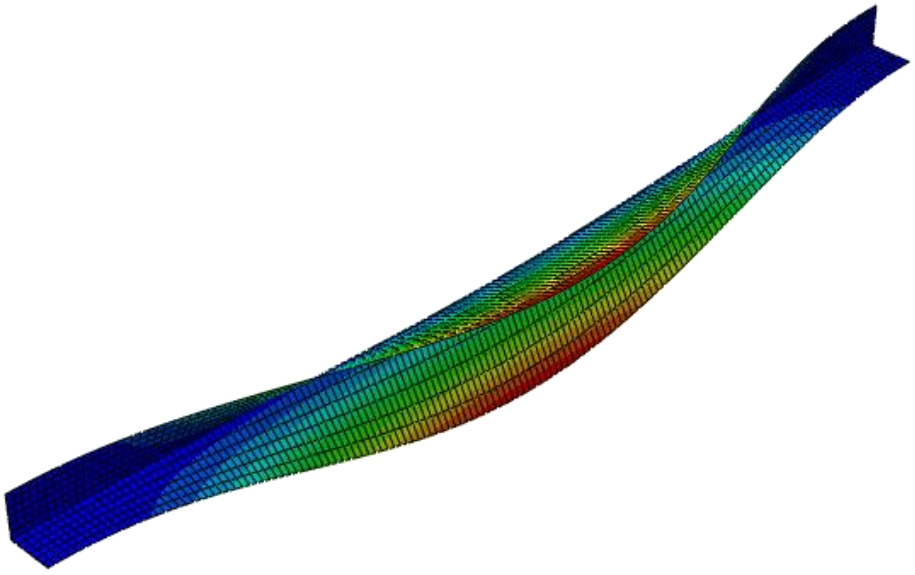

Figure 14. Local failure mode, L=1500 mm

In order to observe a global buckling mode, a bigger thickness was assumed (t=20mm), and it was correctly achieved, as shown in Figures 15 and 16.

- L=500 mm

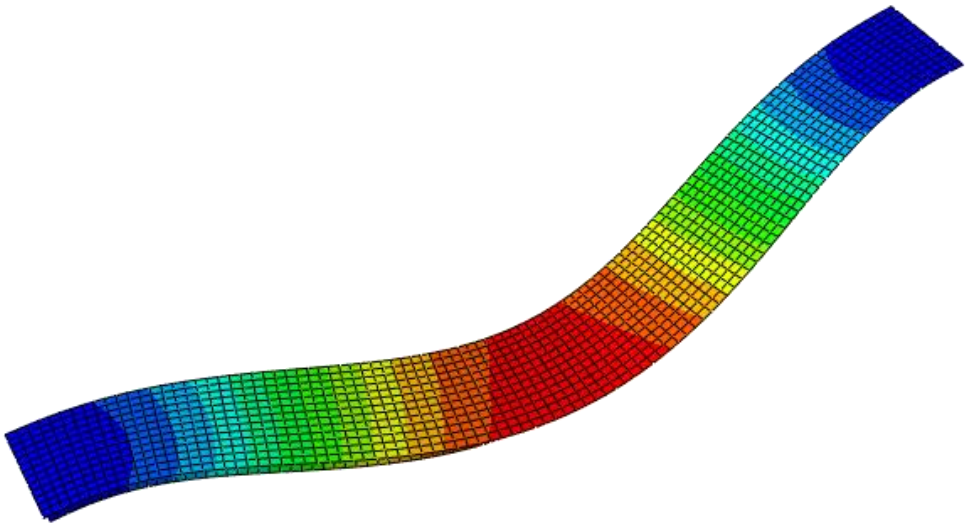

Figure 15. Overall failure l mode, L=500

- L=1500 mm

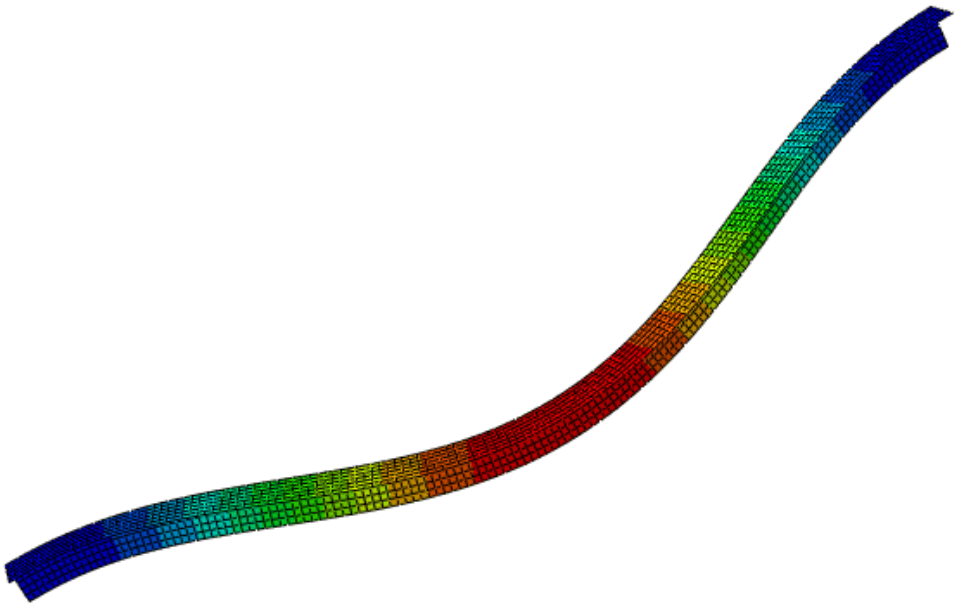

Figure 16. Overall failure mode, L=1500 mm

The local buckling modes were incorporated into the Static, Riks analysis as initial imperfections of the two specimens, with the amplitudes equal to: t/10 (according to Lendesmann et al. (2017)), and 1.024 (0.8b/50), where t is the thickness of the cross-section and b is the width (Jandera and Zhang, 2017). The global buckling modes were also incorporated into the analysis for both of the members as initial imperfections with different amplitudes.

The results of the Riks analysis (with initial geometric imperfections added), are discussed next, the behavior of each element with the used amplitudes is shown in Figures 17 and 18.

For the short member (L=500 mm), the amplitude that showed a more adequate behavior when only global imperfections were taking into account was L/300 (see Figure 18), this was observed after making a study using different amplitudes, and the shape of the curve was identically to the curve PAPER. However, for this specimen, the best result was obtained with the local buckling mode using the amplitude of t/10 and the shape of the obtained curve is also similar to one of the experimental curves (PAPER2) as shown in Figure 17. There is also the option of combining the two types of imperfections derived from the different buckling modes, tested with three different combinations, COMB: Global L/300 and Local t/10, COMB2: L/360, 1.024 (0.8b/50), COMB3: L/678 and t/10. The more accurate result was achieved with COMB3. See Figures 17 and 18 where the experimental

and numerical load-end shortening curves are presented for the different imperfections considered in the analysis.

In Table 5, the values of the ultimate loads and corresponding end-shortenings from the experimental test and FE model are shown, as well as the ratio P_{model}/P_{exp}.

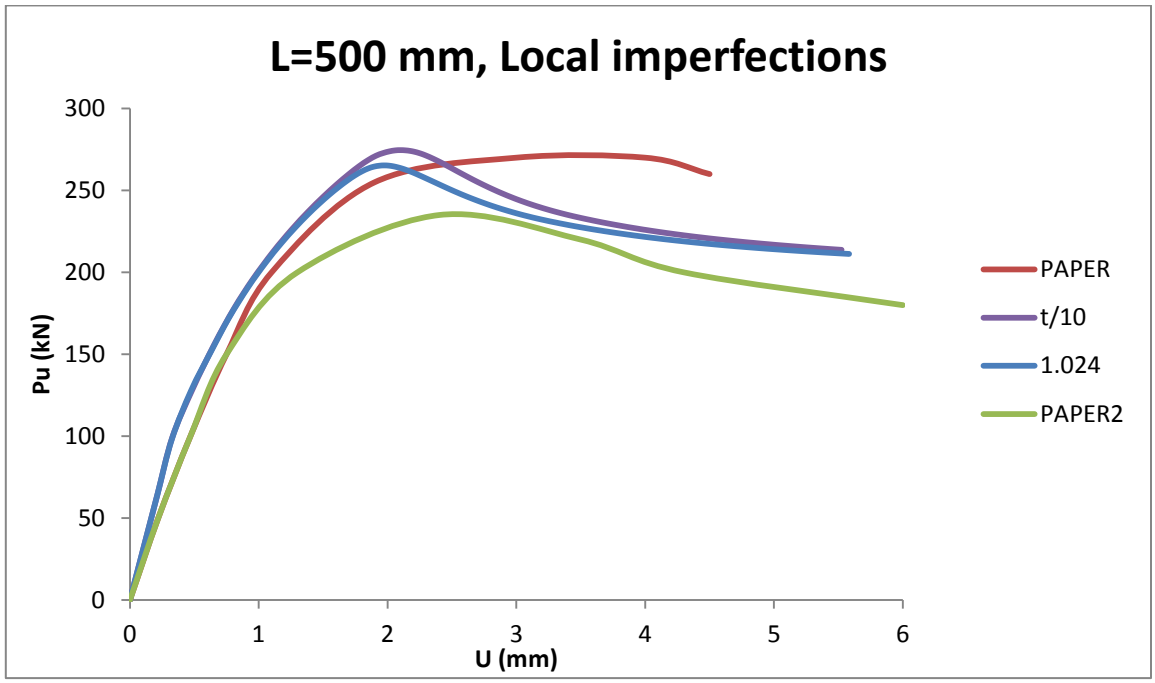

Figure 17. Local buckling mode as initial imperfection in short member

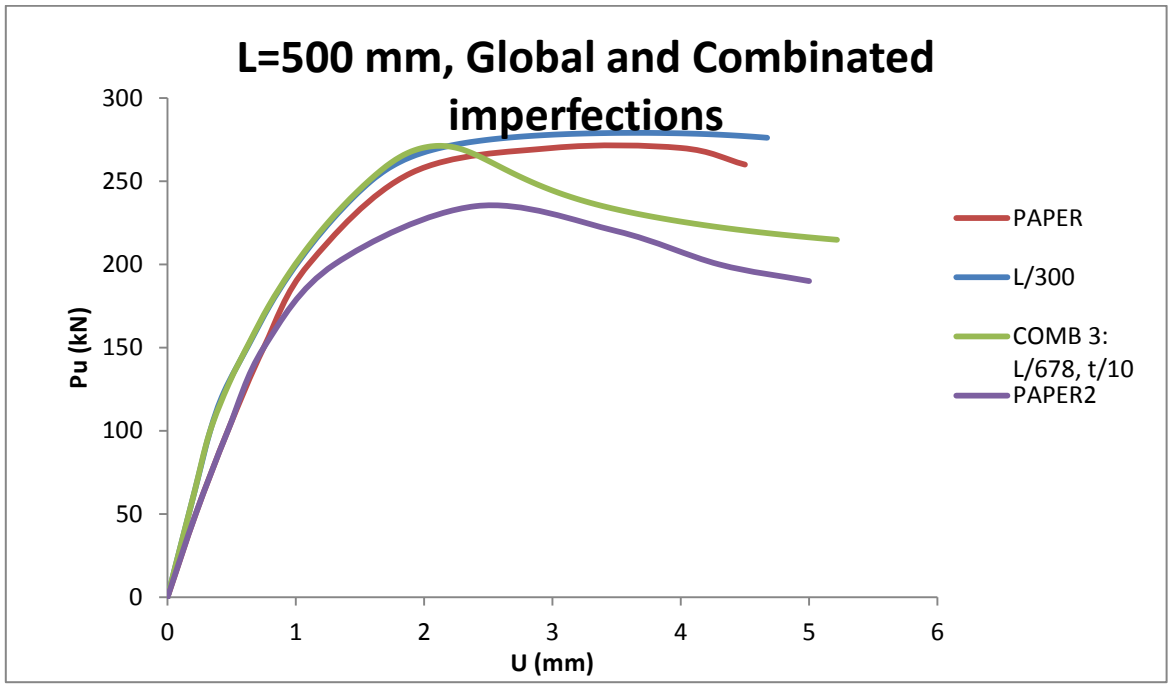

Figure 18. Global and combined buckling mode as initial imperfection in short member

Table 5. Ultimate loads for experimental test and FE model, L=500 mm

OVERALL IMP	**Exp**	**L/300**	**L/678, t/10**
P_u (kN)	272.4	279.1	271.3
U (mm)	3.5	3.57	2.111
P_{model}/P_{exp}		1.02	1.00
LOCAL IMP	**Exp**	**1.024**	**t/10**
P_u (kN)	272.4	265.3	274.6
U (mm)	3.5	1.97	2.099
P_{model}/P_{exp}		0.97	1.01

After analyzing Table 5 it is possible to observe that the failure loads (P_{model}), are very close to the experimental ones since all P_{model}/P_{exp} ratios are verge to 1.

For the considered long member (L=1500 mm) the amplitude that showed the more accurate behavior was L/1000, where L is the overall column length, as shown in Figure 19 and Table 6. This amplitude was also chosen after making a study with different values. Using only the local buckling mode the results were not accurate, as expected, because of the length of the specimen the determining buckling mode is the overall one.

However with a combination of local and overall modes similar results were obtained (COMB: L/1000, t/10) see Figure 19. The difference in the stiffness of the curve could be due to the different levels of restrain in the FE model and during the test. While in the FE analysis a perfect fixation of the column was modeled, this did not occur during the tests according to the authors. In Table 6 the values of the experimental test and FE model are shown, also the ratio P_{model}/P_{exp}.

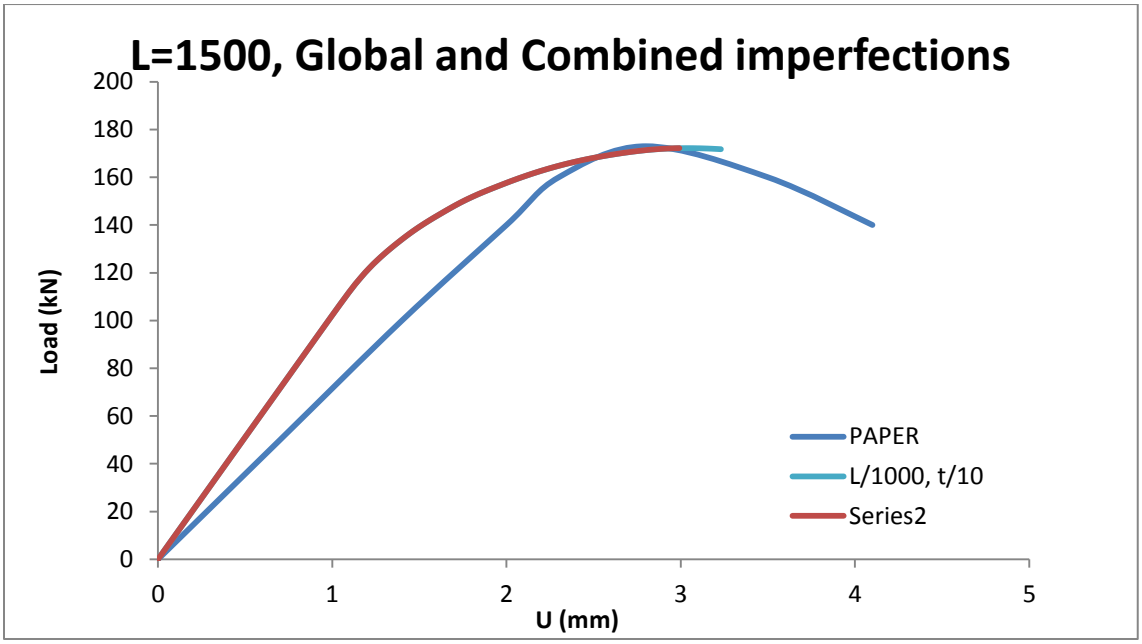

Figure 19. Global and combined buckling mode as initial imperfection in long member

Table 6. Ultimate loads for experimental test and FE model, L=1500 mm

GLOBAL IMP	**Exp**	**L/1000**	**L/1000, t/10**
P_u (kN)	172.8	172.2	172.6
U (mm)	2.8	3.08	3.074
P_{model}/P_{exp}		1.00	1.00
LOCAL IMP	**Exp**	**t/10**	
P_u (kN)	172.8	181	
U (mm)	3.5	2.099	
P_{model}/P_{exp}		0.66	

In Table 6 it is also possible to observe that the P_{model}/P_{exp} ratio are very close to 1, which indicates the proximity of the numerical model with the experimental tests, and validates it.

3.3.2 Lendesmann et al. (2017) validation model

1. Cross-Section:

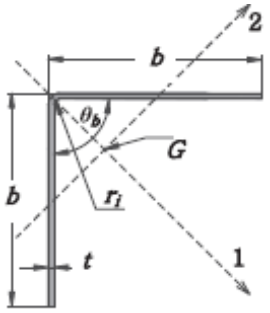

Figure 20. Studied cross-section (Lendesmann et al., 2017)

Dimensions: 50x50x1.55 (mm)
Studied Lengths: 600, 900 (mm)

2. Test configuration: the columns were tested under pure compression to determine the capacity of the angle section members. The support conditions of the columns were fixed with respect to major-axis buckling and torsion, and pinned with respect to minor-axis buckling, preventing transverse displacements and major-axis buckling and torsional rotations as specified in the experimental setup (see Figures 21 and 22).

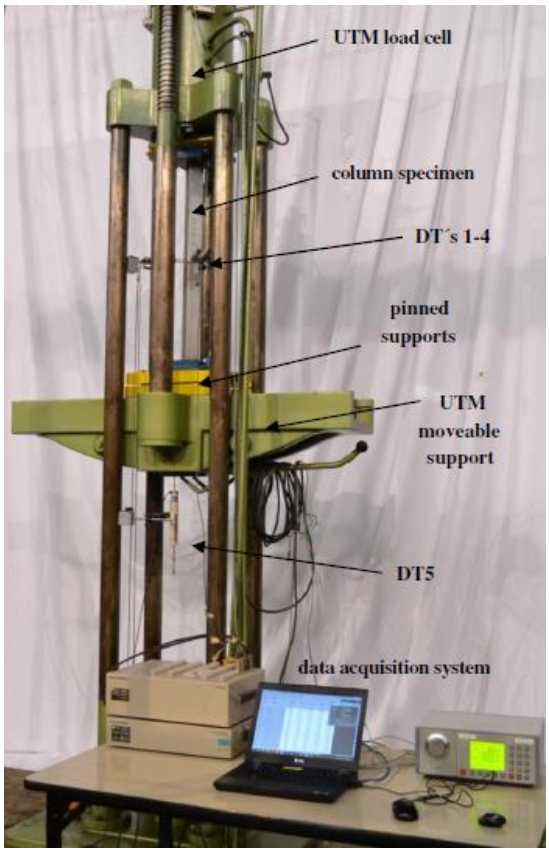

Figure 21. Experimental setup (Lendesmann, et al. 2017)

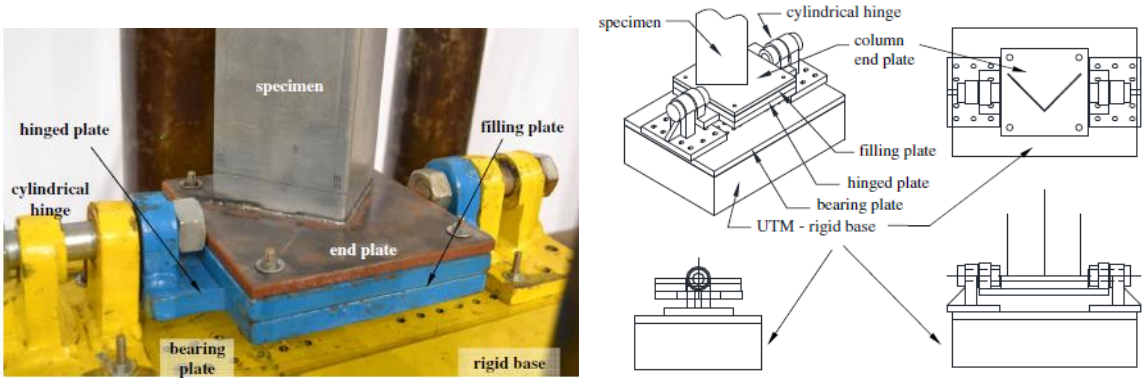

Figure 22. Diagrams of the experimental setup (Lendesmann, et al. 2017)

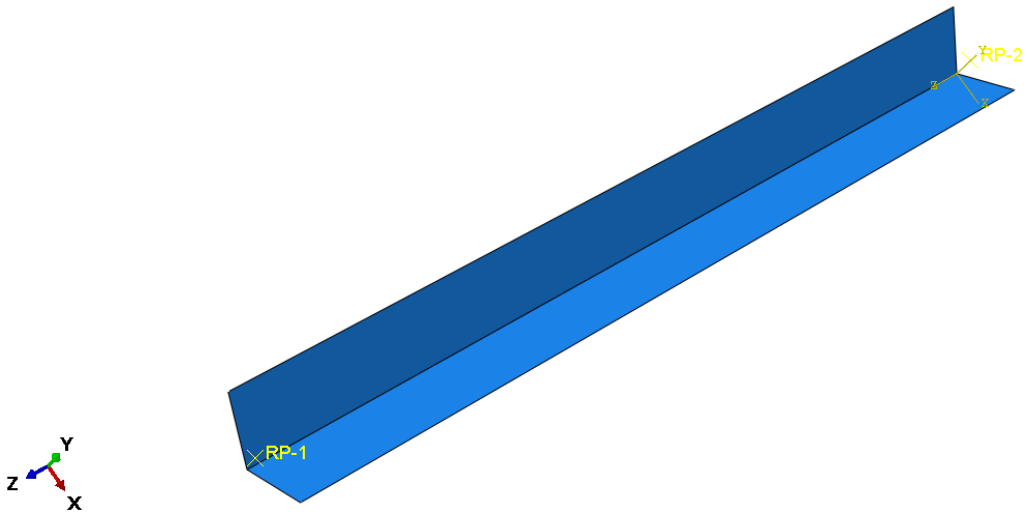

Figure 23. FE model

The two reference points (RP1 and RP2) were placed at the centroid of the cross-section, 12 mm away from the ends of the column as shown in Figure 23, replicating the experimental setup since in the test configuration two knife edges were used to allow minor axis rotations at both ends.

The border conditions of the model consisted in restraining all movements and all rotations except the rotation along the v axis as the test configuration shows (x axis in Abaqus, see Figure 24). As mentioned before, an imposed displacement at the top of the column was applied to simulate the applied force in the member.

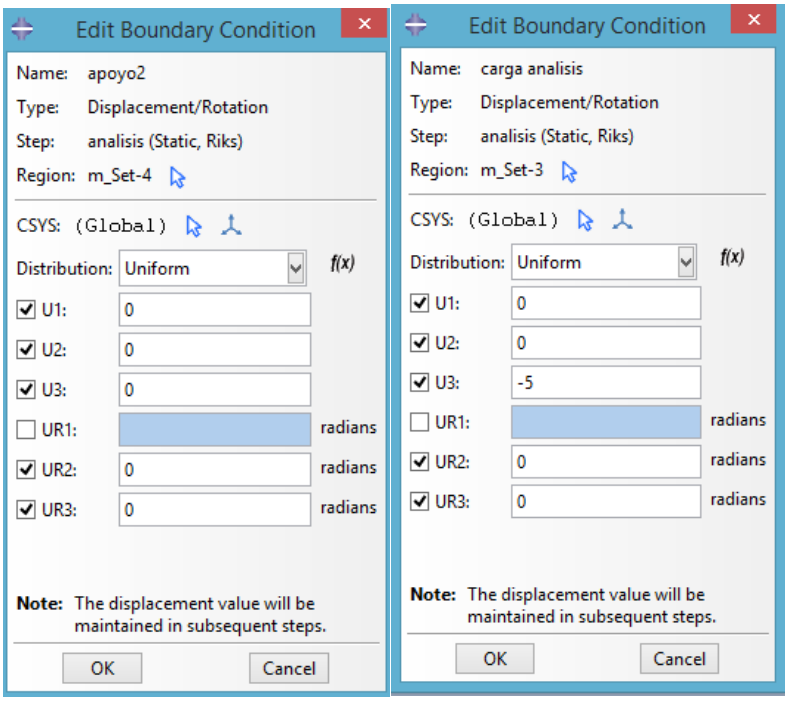

Figure 24. Border conditions applied in the FE model

3. Material

The material used in this experimental program was carbon steel (ZAR-345), after making the tensile coupon tests the average values were obtained and reported in the paper, and are shown in Table 7, while in Figure 25 the stress-strain curve is depicted.

Table 7. Material parameters for the FE model validation

Carbon steel	
f_y (MPa)	304.5
f_u (MPa)	376.1
E (MPa)	205000

Where:

f_y is the yield strength

f_u is the ultimate strength

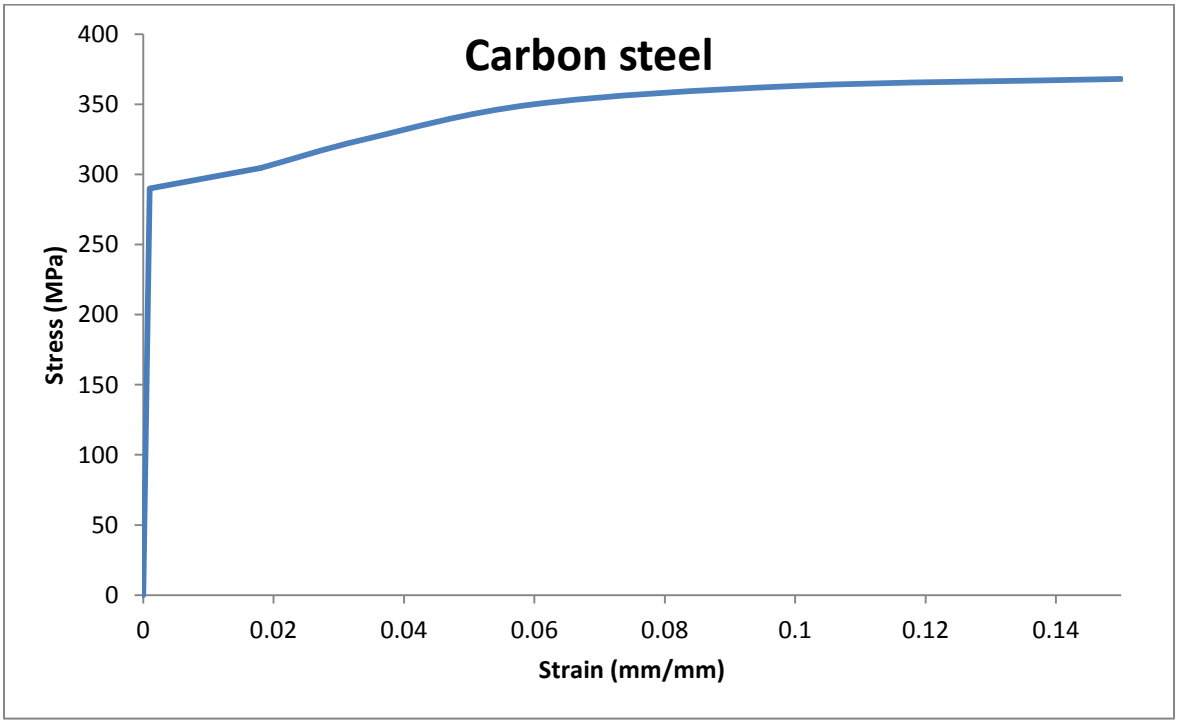

Figure 25. Stress-strain curve of the material

4. Imperfections: as mentioned in the General Assumptions section, a linear buckle analysis was made to determine the buckling modes and eigenvalues. The first buckle analysis was made with the original thickness (t=1.55 mm), and a local mode was obtained for both column lengths, due to the slenderness of the cross-section, as shown in Figures 26 and 27.

- L=600 mm

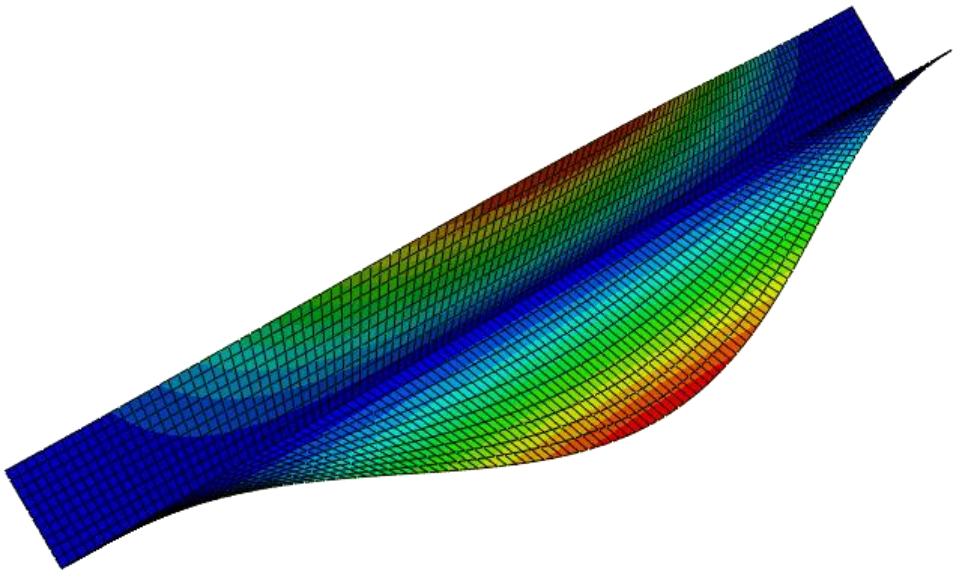

Figure 26. Local failure mode, L=600 mm

- L=900 mm

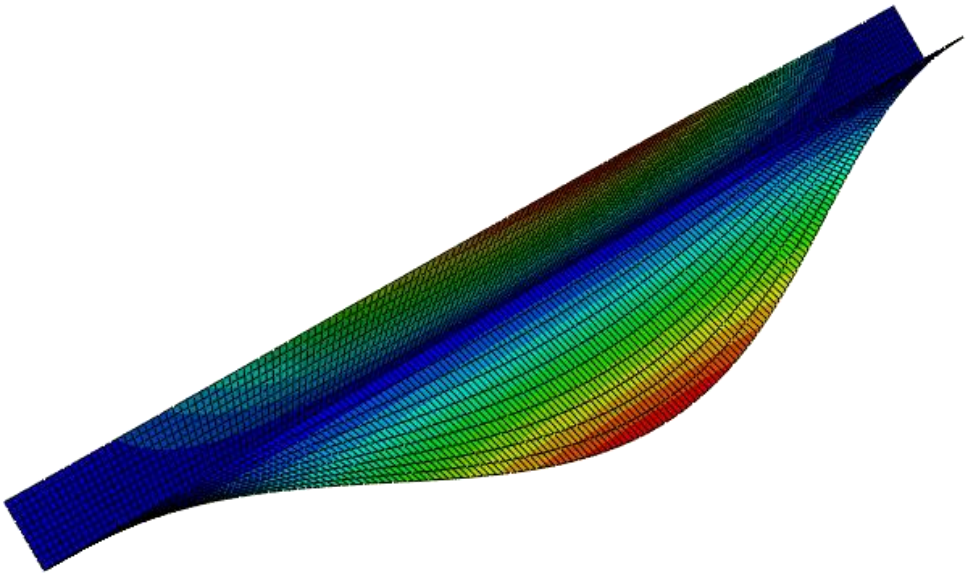

Figure 27. Local failure mode, L=900 mm

In order to obtain an overall buckling mode to be introduced as a global imperfection, a bigger thickness was assumed (t=10 mm), and it was correctly achieved for both considered column lengths, as shown in Figures 28 and 29.

- L=600 mm

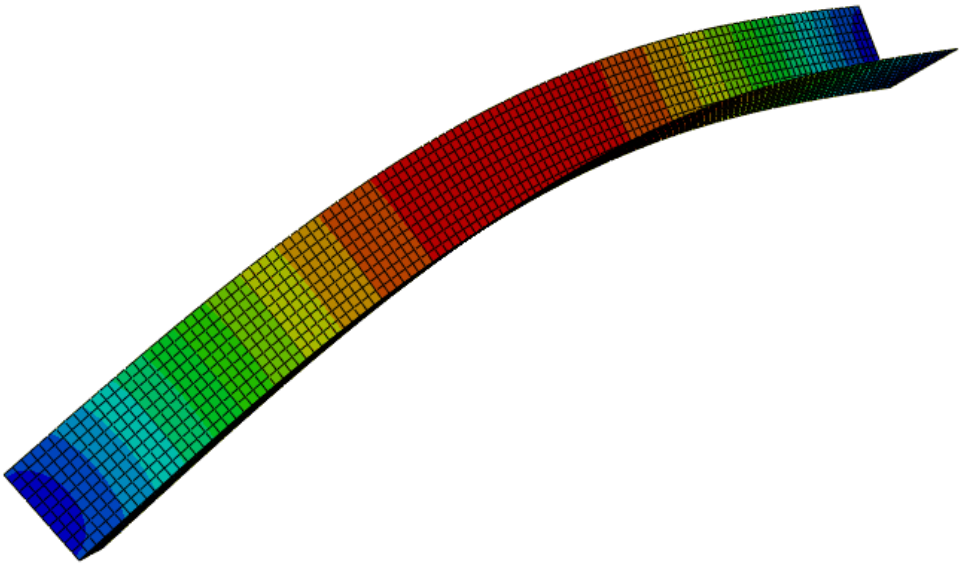

Figure 28. Overall failure mode, L=600 mm

- L=900 mm

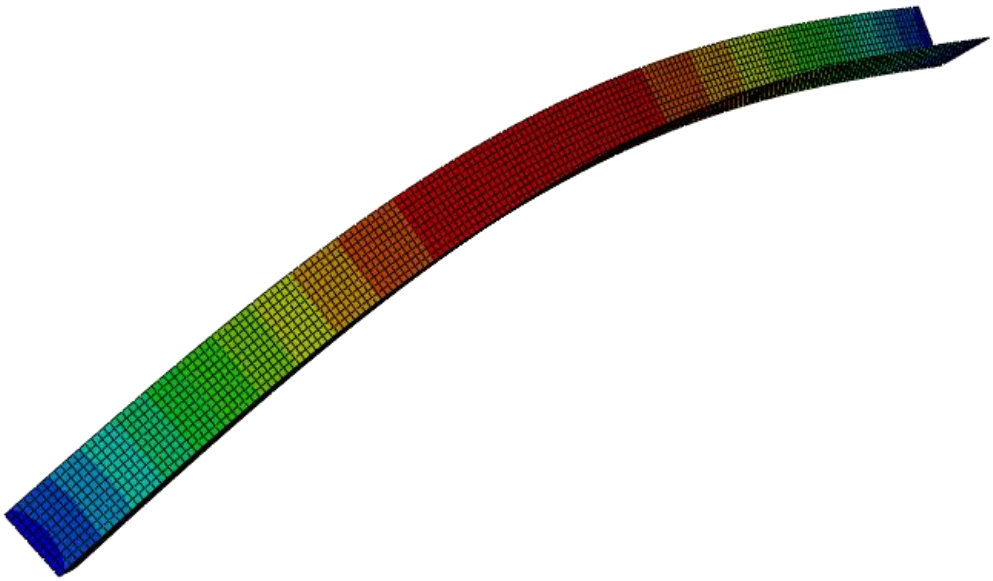

Figure 29. Overall failure mode, L=900 mm

The local buckling mode was incorporated into the Static, Riks analysis as initial imperfections of the two members, with the amplitudes: t/10 and t/50. The global buckling

mode was also incorporated into the analysis as initial imperfections of the member, for the both columns with the amplitudes L/750 and L/1000.

For the short specimen (L=600 mm) the best result was obtained combining the global and local buckling mode (COMB) using amplitudes of L/1000 and t/10 respectively, also the shape of the curve is similar to one of the experimental curves, see Figure 30. With a global buckling mode as initial imperfection the results are not accurate, since the ultimate load is much higher compared to the experimental one. This is due to the slender nature of the studied cross-section, which makes necessary the consideration of local imperfections in the FE analysis. In Table 8 the values of the experimental test and FE model are shown, also the ratio P_{model}/P_{exp}.

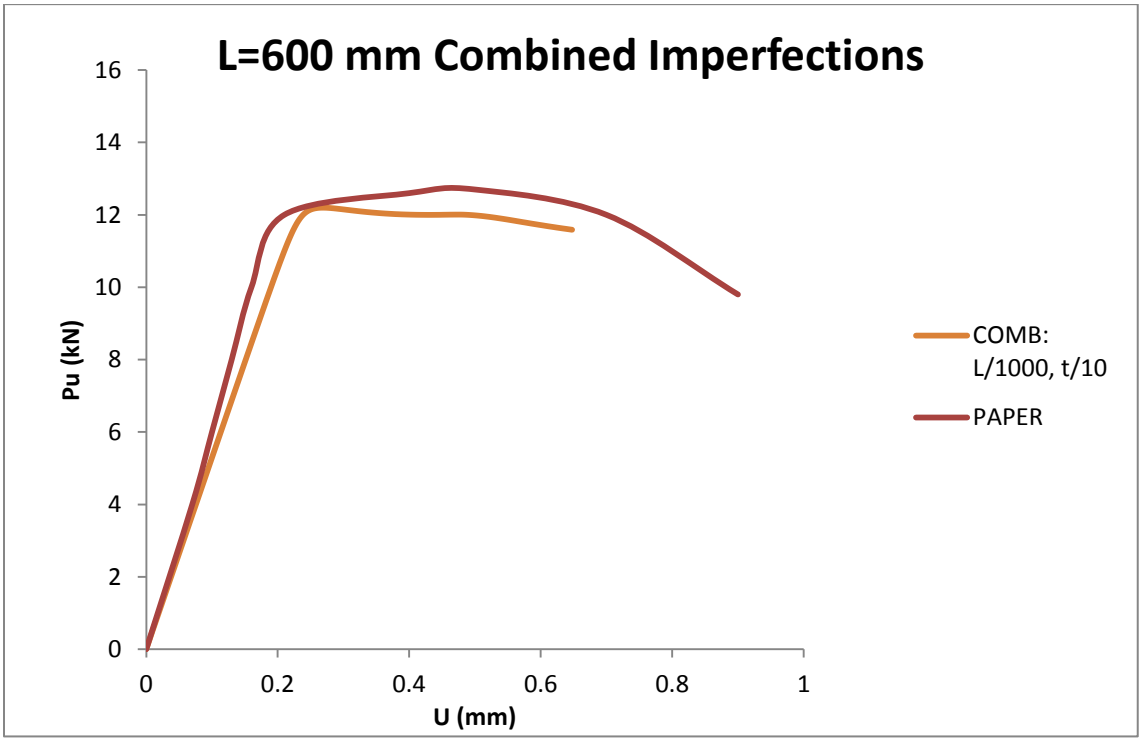

Figure 30. Local and combined buckling mode as initial imperfection in L=600 mm

Table 8. Ultimate loads for experimental test and FE model, L=600 mm

GLOBAL IMP	**Exp**	**L/1000**	**L/750**
P_u (kN)	13.3	37.0	40.5
U (mm)	0.3	0.70	1.72
P_{model}/P_{exp}		2.78	3.04
LOCAL IMP	**Exp**	**L/1000, t/10**	
P_u (kN)	13.3	12.2	
U (mm)	0.3	0.268	
P_{model}/P_{exp}		0.92	

For the long specimen (L=900 mm) the best results are obtained combining the local and global imperfections, as for the short member, with the amplitudes of t/10 and L/1000 respectively. In Table 9 the values of the experimental test and FE model are shown, also the ratio P_{model}/P_{exp}. In the paper there was no curve for the long specimen, therefore the curves cannot be compared.

Table 9. Ultimate loads for experimental test and FE model, L=900 mm

GLOBAL IMP	**Exp**	**L/1000**	**L/750**
P_u (kN)	11.4	31.5	29.8
U (mm)	-	0.895	0.923
P_{model}/P_{exp}		2.76	2.61
LOCAL IMP	**Exp**	**t/10**	**L/1000, t/10**
P_u (kN)	11.4	10.8	11.7
U (mm)	-	0.337	0.320
P_{model}/P_{exp}		0.95	1.03

Therefore, it can be concluded that the conducted FE models accurately capture the stiffness and general shape of the response of specimens, and the obtained failure modes are also found to be in good agreement with those observed after the tests.

3.4 Parametric study

Once the validation of the models was completed, the parametric study was carried out covering the practical ranges of overall slenderness values and cross-sectional slenderness values, fulfilling the objective of this work: to study the structural behavior of equal-leg angle sections subjected to compression.

Once again ABAQUS was used in the numeral simulations.

A total of 162 columns were studied, corresponding to all combinations of 6 cross-section geometries, 9 member slenderness and 3 different materials (which represent basic austenitic, ferritic and duplex stainless steel grades).

3.4.1 Overall slenderness

The overall slenderness of stainless steel columns is commonly defined as shown in Eq. (20) (EN1993-1-4, 2006). In this study the values of these slenderness varied between [0.15, 3], consequently the lengths of the studied members varied between [100, 6900] mm.

$$\bar{\lambda} = \frac{L}{\pi} * \sqrt{\frac{A * \sigma_{0.2}}{E * I}} \tag{20}$$

The values of the non-dimensional slenderness are shown in Table 10.

Table 10. Values of the non-dimensional slenderness considered in parametric studies

$\bar{\lambda}$
0.15
0.25
0.5
0.75
1
1.5
2
2.5
3

3.4.2 Geometry

The geometry of each cross-section was chosen according to their local slenderness, in order to choose only cross-section classified as class 3. This verification was made as specified in EN1993-1-4+A1:2015 as follows:

$$\frac{h}{t} \leq 15\varepsilon; \frac{b+h}{2t} \leq 11.5\varepsilon \tag{21}$$

All the considered cross-sections were fully effective so the interaction of local buckling with flexural and torsional-flexural buckling did not occur, and minor axis behavior of the member was investigated. This allowed the buckling curves to be studied without considering the effect of local buckling, which should be incorporated in a future study.

The cross-section studied in this work is shown in Figure 31.

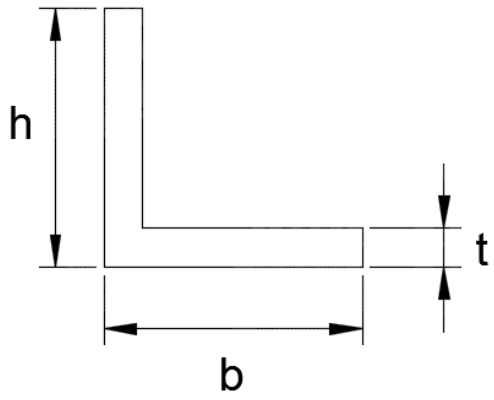

Figure 31. Cross-section studied in the parametric study

The range of the widths of the cross-sections considered in the parametric study varied between 40 mm and 140 mm in order to represent sections with cross-sections dimensions commonly used in practice with widely different characteristics (stocky

sections, slender sections) demonstrating how different sections affect the structural behavior of angle columns. The cross-sections that were studied in this work are shown in Table 11. Note that for each of these 6 cross-sections, 9 different slenderness have been evaluated, for all 3 different materials.

Table 11. Studied cross-section

Cross-section	
b=h (mm)	**t (mm)**
40	6
65	10
80	10
100	12
120	14
140	16

3.4.3 Material

As mentioned above, in this work 3 different stainless steel grades were considered, representing basic austenitic, duplex and ferritic stainless steel grades. These grades were chosen because of their wide and common use in structures.

The basic material properties were taken from Afshan et al., (2017) called: Standardised Material Properties for Numerical Parametric Studies of Structural Stainless Steel Elements, where a wide study was made centered on the analysis of an extensive data base of stainless steel material stress-strain curve results, collected from the literature.

The material properties for hot-rolled angle sections are shown in Table 12 (Afshan et al., 2017). In Figure 32 the stress-strain curves for all 3 materials is shown.

Table 12. Basic material properties for austenitic, duplex and ferritic stainless steels considered in the parametric study

AUSTENITIC	
E (MPa)	200000
$\sigma_{0,2}$ (MPa)	280
n	9.1
E_y (MPa)	14286
σ_u (MPa)	580
ε_u	0.5
m	2.3

DUPLEX	
E (MPa)	200000
$\sigma_{0,2}$ (MPa)	530
n	9.3
E_y (MPa)	24941
σ_u (MPa)	770
ε_u	0.3
m	3.6

FERRITIC	
E (MPa)	200000
$\sigma_{0,2}$ (MPa)	320
n	17.2
E_y (MPa)	8889
σ_u (MPa)	480
ε_u	0.16
m	2.8

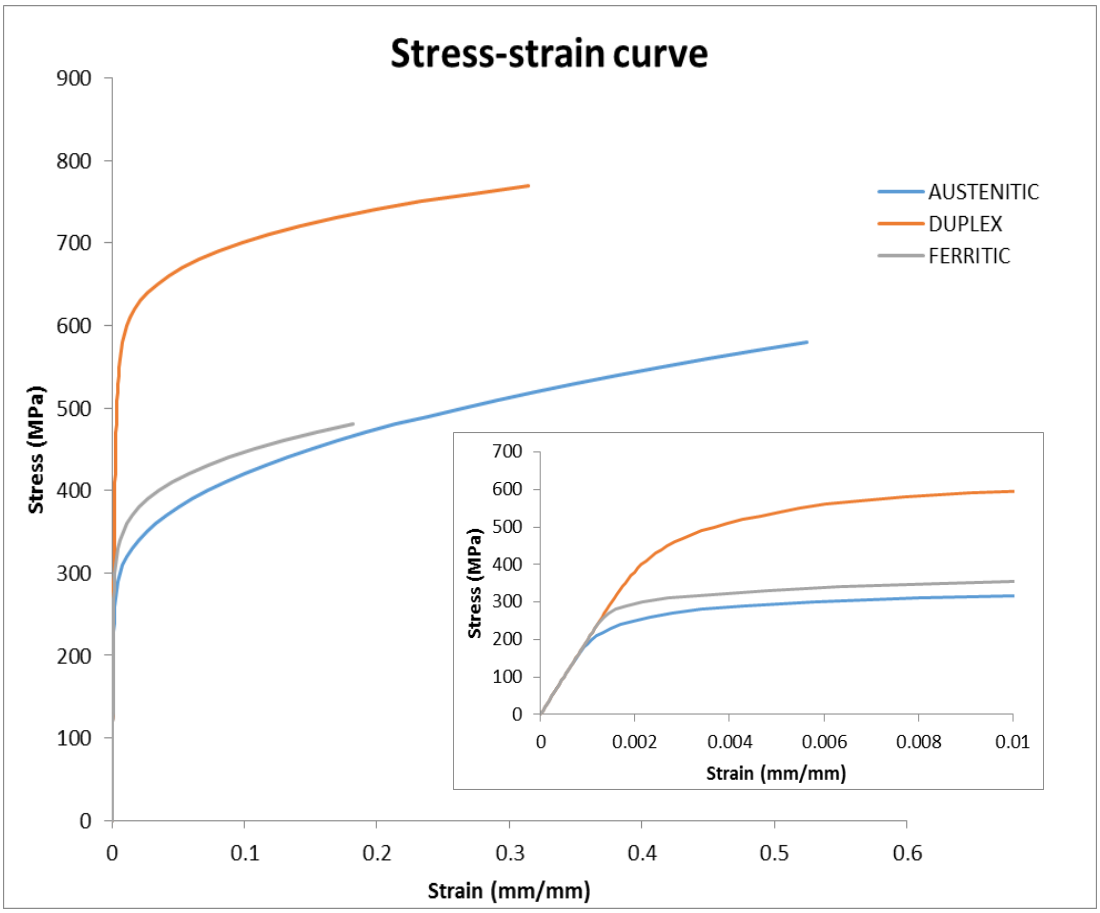

Figure 32. Stress-strain curve for the austenitic, duplex and ferritic stainless steels considered in the parametric study

3.4.4 Summary of specimens

In Table 13 all the sections that were studied in this work are shown, along with the lengths and slenderness for each case.

Table 13. Members studied in numerical simulation

Cross-section		Austenitic		Ferritic		Duplex	
b=h (mm)	t (mm)	L (mm)	$\bar{\lambda}$	L (mm)	$\bar{\lambda}$	L (mm)	$\bar{\lambda}$
40	6	100	0.15	100	0.16	70	0.15
		150	0.23	150	0.24	120	0.25
		300	0.46	300	0.49	250	0.53
		500	0.76	450	0.73	350	0.74
		650	0.99	600	0.98	450	0.95
		1000	1.53	900	1.47	700	1.47
		1300	1.99	1250	2.04	950	2.00
		1650	2.52	1550	2.53	1200	2.52
		1950	2.98	1800	2.94	1400	2.94
65	10	150	0.14	150	0.15	100	0.13
		250	0.24	250	0.25	200	0.26
		550	0.52	500	0.50	350	0.45
		800	0.75	750	0.75	550	0.71
		1050	0.99	1000	1.01	750	0.97
		1600	1.50	1500	1.51	1150	1.49
		2150	2.02	2000	2.01	1550	2.01
		2650	2.49	2450	2.46	1950	2.52
		3150	2.96	2950	2.97	2300	2.98
80	10	200	0.15	200	0.16	150	0.16
		350	0.27	350	0.28	250	0.26
		650	0.49	650	0.53	450	0.47
		1000	0.76	1000	0.81	700	0.73
		1300	0.99	1300	1.06	950	0.99
		2000	1.52	2000	1.63	1450	1.52
		2650	2.02	2650	2.16	1900	1.99
		3300	2.51	3300	2.69	2400	2.51
		3950	3.01	3650	2.97	2850	2.98
100	12	250	0.15	250	0.16	200	0.17
		400	0.24	400	0.26	300	0.25
		850	0.52	850	0.55	600	0.50
		1250	0.76	1250	0.81	900	0.75
		1650	1.00	1650	1.07	1200	1.00
		2450	1.49	2450	1.59	1800	1.51
		3300	2.01	3300	2.15	2400	2.01
		4100	2.49	4100	2.67	3000	2.51
		4950	3.01	4600	2.99	3500	2.93

Cont. Table 13. Members studied in numerical simulation

Cross-section		Austenitic		Ferritic		Duplex	
b=h (mm)	t (mm)	L (mm)	$\bar{\lambda}$	L (mm)	$\bar{\lambda}$	L (mm)	$\bar{\lambda}$
120	14	300	0.15	300	0.16	200	0.14
		500	0.25	500	0.27	350	0.24
		950	0.48	950	0.51	700	0.49
		1500	0.76	1500	0.81	1050	0.73
		1950	0.99	1950	1.06	1450	1.01
		2950	1.49	2950	1.60	2150	1.50
		3950	2.00	3950	2.14	2850	1.99
		4950	2.51	4950	2.68	3600	2.51
		5900	2.99	5550	3.01	4300	3.00
140	16	350	0.15	350	0.16	250	0.15
		600	0.26	600	0.28	400	0.24
		1150	0.50	1150	0.53	850	0.51
		1750	0.76	1750	0.81	1250	0.75
		2300	1.00	2300	1.07	1650	0.99
		3450	1.50	3450	1.60	2500	1.49
		4600	2.00	4600	2.13	3350	2.00
		5750	2.50	5750	2.67	4200	2.51
		6900	3.00	6450	2.99	5050	3.02

3.4.5 Imperfections

In Lendesmann et al, (2017), a numerical study was conducted and was validated with experimental tests to determine that the initial geometric imperfections that were incorporated were the combination of a critical flexural-component, with amplitude 0.1t and a non-critical minor-axis flexural component, with amplitude L/1000.

Therefore the amplitudes that were taken into account for the analyses were: L/1000 for global imperfections and t/10 for local imperfections.

As for the validation study, the deformed buckled shape was obtained with a linear buckling analysis and added as an initial geometric imperfection in the non-linear analysis. Therefore, for short specimens the buckling mode that prevailed was the local buckling failure mode, while for longer specimens the global buckling mode was more relevant.

In Table 14 the buckling mode associated with each length is shown.

Table 14. Buckling modes according to the length of the member for each specimen

Cross-section		Austenitic		Ferritic		Duplex	
b=h (mm)	t (mm)	L (mm)	Buckling mode	L (mm)	Buckling mode	L (mm)	Buckling mode
40	6	100	Local	100	Local	70	Local
		150	Local	150	Local	120	Local
		300	Global	300	Global	250	Global
		500	Global	450	Global	350	Global
		650	Global	600	Global	450	Global
		1000	Global	900	Global	700	Global
		1300	Global	1250	Global	950	Global
		1650	Global	1550	Global	1200	Global
		1950	Global	1800	Global	1400	Global
65	10	150	Local	150	Local	100	Local
		250	Local	250	Local	200	Local
		550	Global	500	Global	350	Local
		800	Global	750	Global	550	Global
		1050	Global	1000	Global	750	Global
		1600	Global	1500	Global	1150	Global
		2150	Global	2000	Global	1550	Global
		2650	Global	2450	Global	1950	Global
		3150	Global	2950	Global	2300	Global
80	10	200	Local	200	Local	150	Local
		350	Local	350	Local	250	Local
		650	Global	650	Global	450	Local
		1000	Global	1000	Global	700	Global
		1300	Global	1300	Global	950	Global
		2000	Global	2000	Global	1450	Global
		2650	Global	2650	Global	1900	Global
		3300	Global	3300	Global	2400	Global
		3950	Global	3650	Global	2850	Global
100	12	250	Local	250	Local	200	Local
		400	Local	400	Local	300	Local
		850	Global	850	Global	600	Local
		1250	Global	1250	Global	900	Global
		1650	Global	1650	Global	1200	Global
		2450	Global	2450	Global	1800	Global
		3300	Global	3300	Global	2400	Global
		4100	Global	4100	Global	3000	Global
		4950	Global	4600	Global	3500	Global

Cont. Table 14. Buckling modes according to the length of the member for each specimen

Cross-section		Austenitic		Ferritic		Duplex	
b=h (mm)	t (mm)	L (mm)	Buckling mode	L (mm)	Buckling mode	L (mm)	Buckling mode
120	14	300	Local	300	Local	200	Local
		500	Local	500	Local	350	Local
		950	Global	950	Global	700	Local
		1500	Global	1500	Global	1050	Global
		1950	Global	1950	Global	1450	Global
		2950	Global	2950	Global	2150	Global
		3950	Global	3950	Global	2850	Global
		4950	Global	4950	Global	3600	Global
		5900	Global	5550	Global	4300	Global
140	16	350	Local	350	Local	250	Local
		600	Local	600	Local	400	Local
		1150	Global	1150	Global	850	Local
		1750	Global	1750	Global	1250	Global
		2300	Global	2300	Global	1650	Global
		3450	Global	3450	Global	2500	Global
		4600	Global	4600	Global	3350	Global
		5750	Global	5750	Global	4200	Global
		6900	Global	6450	Global	5050	Global

3.4.6 Boundary conditions

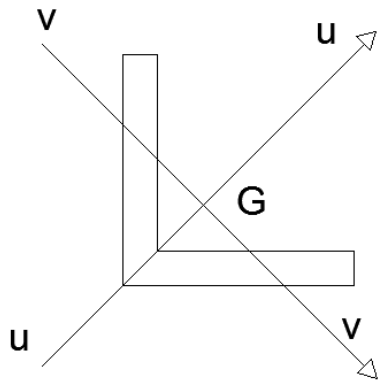

Figure 33. Major and Minor Axis

The boundary conditions for the parametric study were pinned with respect to the minor axis (v-v) and fixed with respect to the major axis (u-u).

Two reference points were positioned at the centroid of the cross-section, and the axial load was applied through one of these points (in terms of displacement). The conditions for

these control points are explained in section 3.2: for one reference point (RP1) all displacements except one was restrained (the displacement along the longitudinal axis), and only rotation around minor axis was permitted. For the other reference point (RP2) all displacements and rotations were restrained except for the rotation around minor axis.

4. BEHAVIOR OF STAINLESS STEEL ANGLE COLUMNS

In the following section the results of the numerical simulations (parametric study) are presented. Therefore, tables with numerical results of the obtained ultimate loads are shown. These results are going to be evaluated and compared with the buckling curve for flexural buckling and torsional flexural buckling, codified in the EN1993-1-4 in order to observe the accuracy of these curves.

Also, two different conditions will be evaluated in this chapter, the influence of the section in the buckling modes, by representing for each material the different sections that were taken into account, and then the influence of the material, by representing in one curve all 3 materials without distinguishing the sections.

4.1 Analysis

The parametric study carried out consisted of 162 FE models on equal-leg angle section columns subjected to flexural buckling, as a result of the combination of 9 overall slenderness values, 6 different geometries (cross-sections) and 3 stainless steel alloys mentioned in section 3.4.

In order to correctly represent the obtained data, it was necessary to determine the failure mode for each section, considering:

$$N_{b,EC} = \min(N_{b,F\ (curve\ d)}, N_{b,FT\ (curve\ b)})$$

where:

$$N_{b,F\ (curve\ d)} \rightarrow Flexural\ \ mode$$

$$N_{b,FT\ (curve\ b)} \rightarrow Flexural\ torsional\ mode$$

According to these expressions and the specified in the EN1993-1-4 (2006) the failure modes were determined analytically, and were compared to the failure modes obtained according to the finite element (FE) analysis. The failure modes obtained in the FE models are shown in Table 15, where F-T means Flexural-Torsional. All failure modes for all cross-sections, lengths and materials obtained analytically matched those obtained in the FE models, except the last four cross-sections of the duplex stainless steel, for the $\bar{\lambda}$ =0.5, where the analytic failure mode was flexural buckling instead of flexural-torsional buckling predicted by the code.

Table 15. FE model failure modes for each specimen

Cross-section		Austenitic		Ferritic		Duplex	
b=h (mm)	t (mm)	$\bar{\lambda}$	Failure mode	$\bar{\lambda}$	Failure mode	$\bar{\lambda}$	Failure mode
40	6	0.15	F-T	0.16	F-T	0.15	F-T
		0.23	F-T	0.24	F-T	0.25	F-T
		0.46	FLEXURAL	0.49	FLEXURAL	0.53	FLEXURAL
		0.76	FLEXURAL	0.73	FLEXURAL	0.74	FLEXURAL
		0.99	FLEXURAL	0.98	FLEXURAL	0.95	FLEXURAL
		1.53	FLEXURAL	1.47	FLEXURAL	1.47	FLEXURAL
		1.99	FLEXURAL	2.04	FLEXURAL	2.00	FLEXURAL
		2.52	FLEXURAL	2.53	FLEXURAL	2.52	FLEXURAL
		2.98	FLEXURAL	2.94	FLEXURAL	2.94	FLEXURAL
65	10	0.14	F-T	0.15	F-T	0.13	F-T
		0.24	F-T	0.25	F-T	0.26	F-T
		0.52	FLEXURAL	0.50	FLEXURAL	0.45	FLEXURAL
		0.75	FLEXURAL	0.75	FLEXURAL	0.71	FLEXURAL
		0.99	FLEXURAL	1.01	FLEXURAL	0.97	FLEXURAL
		1.50	FLEXURAL	1.51	FLEXURAL	1.49	FLEXURAL
		2.02	FLEXURAL	2.01	FLEXURAL	2.01	FLEXURAL
		2.49	FLEXURAL	2.46	FLEXURAL	2.52	FLEXURAL
		2.96	FLEXURAL	2.97	FLEXURAL	2.98	FLEXURAL
80	10	0.15	F-T	0.16	F-T	0.16	F-T
		0.27	F-T	0.28	F-T	0.26	F-T
		0.49	FLEXURAL	0.53	FLEXURAL	0.47	F-T
		0.76	FLEXURAL	0.81	FLEXURAL	0.73	FLEXURAL
		0.99	FLEXURAL	1.06	FLEXURAL	0.99	FLEXURAL
		1.52	FLEXURAL	1.63	FLEXURAL	1.52	FLEXURAL
		2.02	FLEXURAL	2.16	FLEXURAL	1.99	FLEXURAL
		2.51	FLEXURAL	2.69	FLEXURAL	2.51	FLEXURAL
		3.01	FLEXURAL	2.97	FLEXURAL	2.98	FLEXURAL
100	12	0.15	F-T	0.16	F-T	0.17	F-T
		0.24	F-T	0.26	F-T	0.25	F-T
		0.52	FLEXURAL	0.55	FLEXURAL	0.50	F-T
		0.76	FLEXURAL	0.81	FLEXURAL	0.75	FLEXURAL
		1.00	FLEXURAL	1.07	FLEXURAL	1.00	FLEXURAL
		1.49	FLEXURAL	1.59	FLEXURAL	1.51	FLEXURAL
		2.01	FLEXURAL	2.15	FLEXURAL	2.01	FLEXURAL
		2.49	FLEXURAL	2.67	FLEXURAL	2.51	FLEXURAL
		3.01	FLEXURAL	2.99	FLEXURAL	2.93	FLEXURAL

Cont. Table 15. FE model failure modes for each specimen

Cross-section		Austenitic		Ferritic		Duplex	
b=h (mm)	t (mm)	$\bar{\lambda}$	Failure mode	$\bar{\lambda}$	Failure mode	$\bar{\lambda}$	Failure mode
120	14	0.15	F-T	0.16	F-T	0.14	F-T
		0.25	F-T	0.27	F-T	0.24	F-T
		0.48	FLEXURAL	0.51	FLEXURAL	0.49	F-T
		0.76	FLEXURAL	0.81	FLEXURAL	0.73	FLEXURAL
		0.99	FLEXURAL	1.06	FLEXURAL	1.01	FLEXURAL
		1.49	FLEXURAL	1.60	FLEXURAL	1.50	FLEXURAL
		2.00	FLEXURAL	2.14	FLEXURAL	1.99	FLEXURAL
		2.51	FLEXURAL	2.68	FLEXURAL	2.51	FLEXURAL
		2.99	FLEXURAL	3.01	FLEXURAL	3.00	FLEXURAL
140	16	0.15	F-T	0.16	F-T	0.15	F-T
		0.26	F-T	0.28	F-T	0.24	F-T
		0.50	FLEXURAL	0.53	FLEXURAL	0.51	F-T
		0.76	FLEXURAL	0.81	FLEXURAL	0.75	FLEXURAL
		1.00	FLEXURAL	1.07	FLEXURAL	0.99	FLEXURAL
		1.50	FLEXURAL	1.60	FLEXURAL	1.49	FLEXURAL
		2.00	FLEXURAL	2.13	FLEXURAL	2.00	FLEXURAL
		2.50	FLEXURAL	2.67	FLEXURAL	2.51	FLEXURAL
		3.00	FLEXURAL	2.99	FLEXURAL	3.02	FLEXURAL

In Table 16 the overall slenderness and the numerical ultimate flexural buckling load for each section are shown.

Table 16. Overall slenderness and numerical ultimate flexural buckling load for each specimen

Cross-section		Austenitic		Ferritic		Duplex	
b=h (mm)	t (mm)	$\bar{\lambda}$	Pu (kN)	$\bar{\lambda}$	Pu (kN)	$\bar{\lambda}$	Pu (kN)
40	6	0.15	139.47	0.16	155.70	0.15	280.00
		0.23	131.80	0.24	146.13	0.25	254.44
		0.46	104.73	0.49	121.51	0.53	205.28
		0.76	84.28	0.73	107.61	0.74	175.89
		0.99	71.68	0.98	90.41	0.95	149.73
		1.53	41.75	1.47	52.73	1.47	87.22
		1.99	26.51	2.04	29.40	2.00	51.02
		2.52	17.04	2.53	19.61	2.52	32.88
		2.98	12.41	2.94	14.72	2.94	24.46

Cont. Table 16. Non-dimensional slenderness and ultimate buckling load for each specimen

Cross-section		Austenitic		Ferritic		Duplex	
b=h (mm)	t (mm)	$\bar{\lambda}$	Pu (kN)	$\bar{\lambda}$	Pu (kN)	$\bar{\lambda}$	Pu (kN)
65	10	0.14	382.03	0.15	425.62	0.13	739.67
		0.24	353.70	0.25	392.58	0.26	707.05
		0.52	271.04	0.50	326.54	0.45	587.33
		0.75	229.82	0.75	287.91	0.71	484.19
		0.99	194.88	1.01	239.06	0.97	397.08
		1.50	116.05	1.51	137.08	1.49	232.40
		2.02	69.71	2.01	82.19	2.01	137.50
		2.49	47.33	2.46	56.15	2.52	89.35
		2.96	34.09	2.97	39.35	2.98	65.09
80	10	0.15	449.25	0.16	502.10	0.16	858.66
		0.27	432.28	0.28	479.08	0.26	820.22
		0.49	346.69	0.53	405.54	0.47	761.39
		0.76	288.18	0.81	351.21	0.73	601.52
		0.99	246.64	1.06	288.80	0.99	492.93
		1.52	145.01	1.63	153.14	1.52	286.22
		2.02	89.05	2.16	91.62	1.99	177.50
		2.51	59.29	2.69	60.13	2.51	114.42
		3.01	42.13	2.97	49.46	2.98	82.26
100	12	0.15	669.07	0.16	747.80	0.17	1269.22
		0.24	653.05	0.26	739.18	0.25	1222.50
		0.52	513.48	0.55	603.79	0.50	1124.80
		0.76	434.31	0.81	529.49	0.75	893.25
		1.00	367.76	1.07	429.06	1.00	737.24
		1.49	226.38	1.59	239.81	1.51	437.67
		2.01	135.56	2.15	139.72	2.01	263.22
		2.49	90.63	2.67	92.59	2.51	172.97
		3.01	63.37	2.99	74.22	2.93	128.73
120	14	0.15	932.11	0.16	1039.86	0.14	1807.57
		0.25	909.17	0.27	1020.88	0.24	1703.39
		0.48	739.98	0.51	862.65	0.49	1598.48
		0.76	609.89	0.81	743.69	0.73	1273.16
		0.99	522.90	1.06	613.16	1.01	1029.96
		1.49	316.77	1.60	335.44	1.50	620.54
		2.00	191.62	2.14	197.54	1.99	377.63
		2.51	126.12	2.68	128.78	2.51	243.41
		2.99	90.33	3.01	103.34	3.00	173.01

Cont. Table 16. Non-dimensional slenderness and ultimate buckling load for each specimen

Cross-section		Austenitic		Ferritic		Duplex	
b=h (mm)	t (mm)	$\bar{\lambda}$	Pu (kN)	$\bar{\lambda}$	Pu (kN)	$\bar{\lambda}$	Pu (kN)
140	16	0.15	1238.26	0.16	1383.82	0.15	2379.50
		0.26	1206.07	0.28	1363.09	0.24	2262.85
		0.50	975.36	0.53	1141.97	0.51	2109.51
		0.76	814.99	0.81	993.93	0.75	1683.50
		1.00	693.33	1.07	810.70	0.99	1406.37
		1.50	422.21	1.60	446.98	1.49	834.92
		2.00	257.25	2.13	265.23	2.00	498.41
		2.50	170.14	2.67	173.77	2.51	325.70
		3.00	120.32	2.99	139.30	3.02	228.57

As expected with the increase of the cross-section dimensions, the ultimate loads are higher, because of the increase of the inertia (along the minor axis). And with the increase of the slenderness of the members, the ultimate load decrease as specimens get more unstable.

In order to observe the obtained data, in section 4.2 results corresponding to each stainless steel grade considered have been plotted separately with the aim of evaluate the influence of the cross-section in the behavior, and then all stainless steel grades were represented in one curve to appreciate only the influence of the material in the results.

4.2 Comparison of the FE results and the Design Guides

For all stainless steel grades (austenitic, ferritic and duplex), the comparisons with the corresponding buckling curve according to the EN1993-1-4 for the flexural buckling resistance are made (curve d, α=0.76, $\overline{\lambda_o}$=0.2). The same buckling curve is proposed in the DMSSS (2017).

The ultimate buckling load (P_u) that has been obtained with the non-linear analysis shown in Table 16, is used to calculate the numerical reduction factor (χ), as showed in Eq. (22)

$$\chi_{FE} = \frac{P_u}{N_{pl}} \tag{22}$$

Where:

N_{pl} is the design plastic resistance of the cross-section

Then the curve $\bar{\lambda}$ vs χ_{FE} (FE) was created, to compare numerical results to the ones established in the EN1993-1-4, for those speciments showing flexural buckling failure modes (see Table 15).

As said before, results corresponding to each stainless steel grade considered have been plotted separately in order to evaluate the influence of the cross-section in the behavior (see Figures 34, 35 and 36) and then all stainless steel grades were represented in one curve to appreciate only the influence of the material in the results, this is represented in Figure 37.

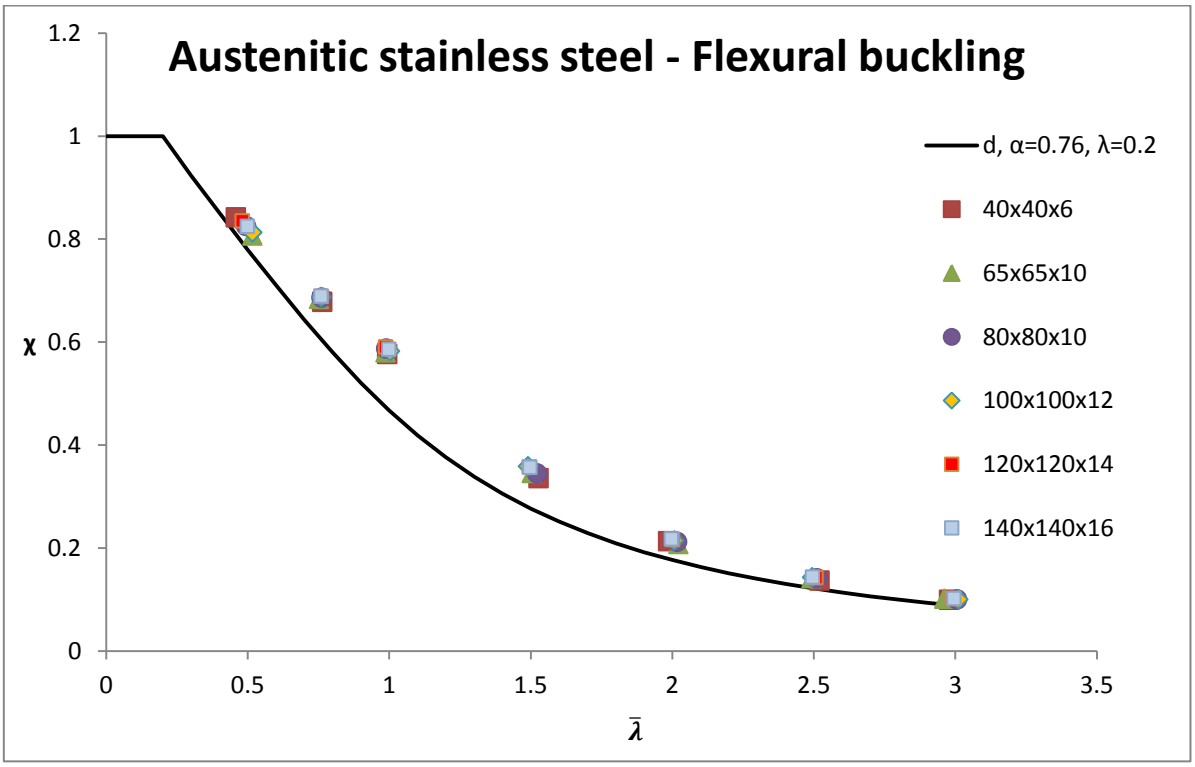

Figure 34. Assessment of the EN1993-1-4 (2006) buckling curve d for austenitic stainless steel angle section members in compression

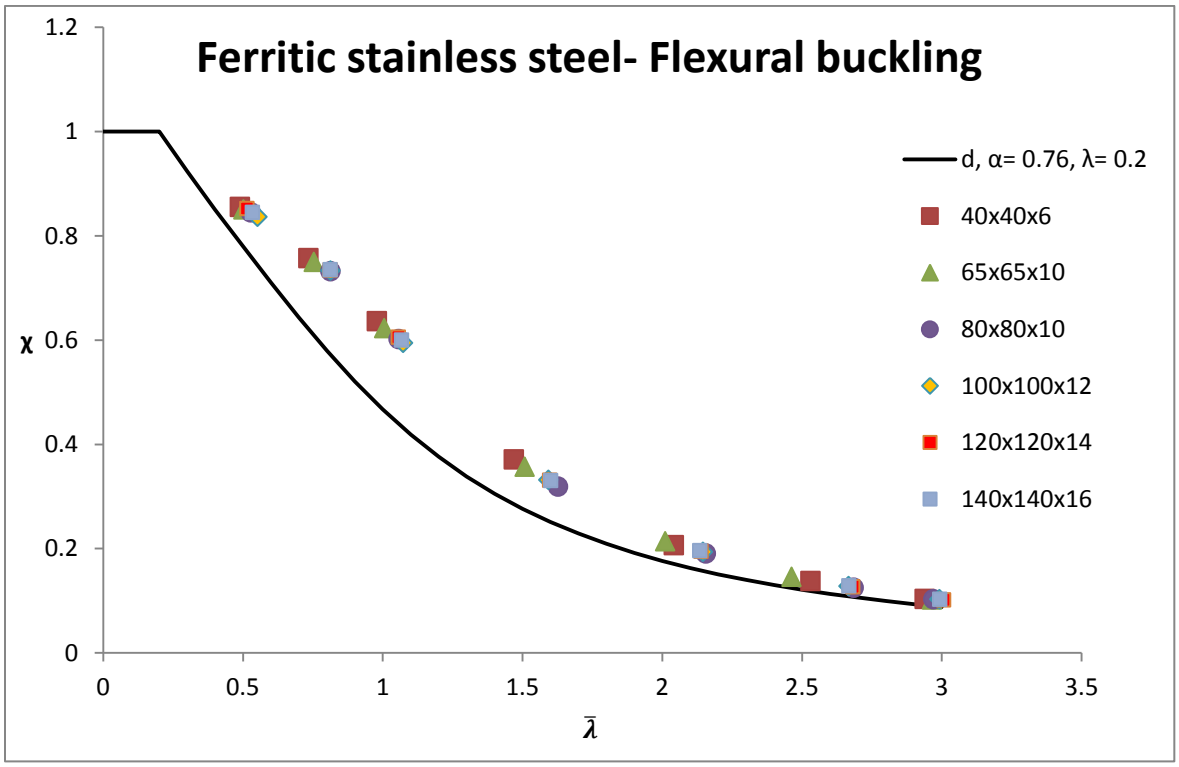

Figure 35. Assessment of the EN1993-1-4 (2006) buckling curve d for ferritic stainless steel angle section members in compression

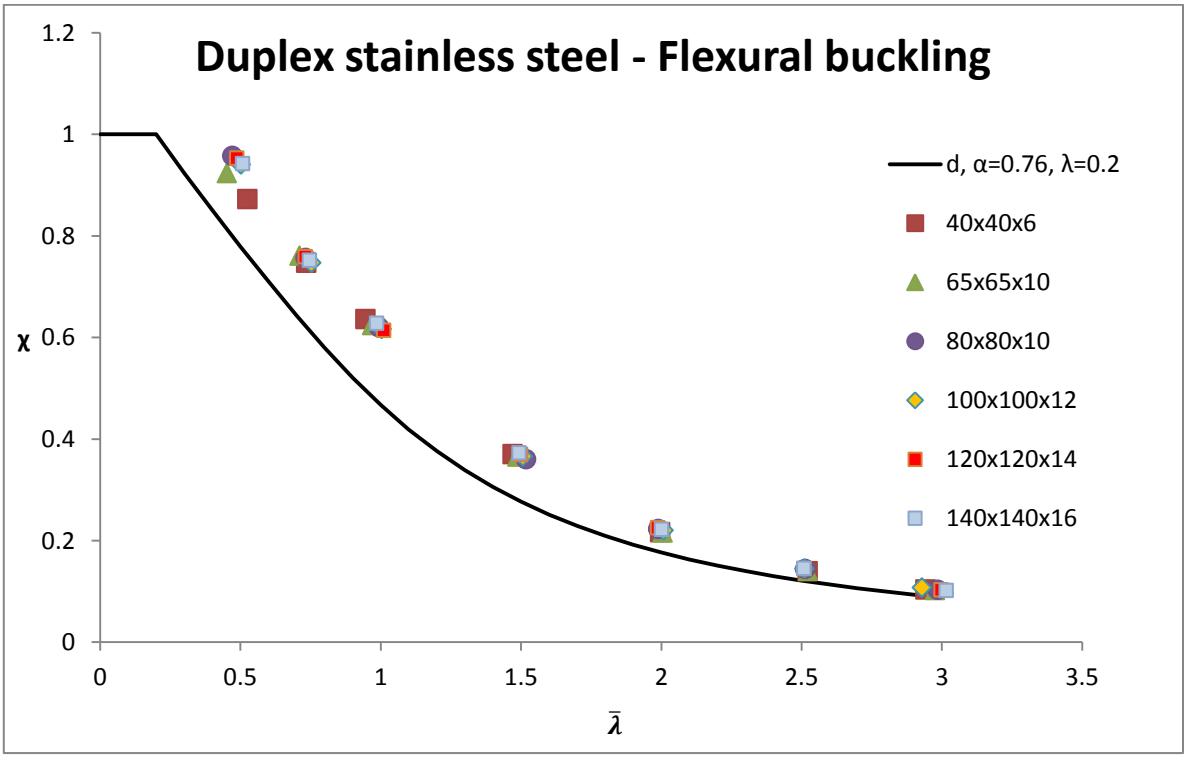

Figure 36. Assessment of the EN1993-1-4 (2006) buckling curve d for duplex stainless steel angle section members in compression

After observing the obtained results for all the stainless steel grades separately, it can be concluded that there is not difference between the different sections that were studied, therefore the behavior does not depend on the dimensions of the cross-section for the chosen ranges.

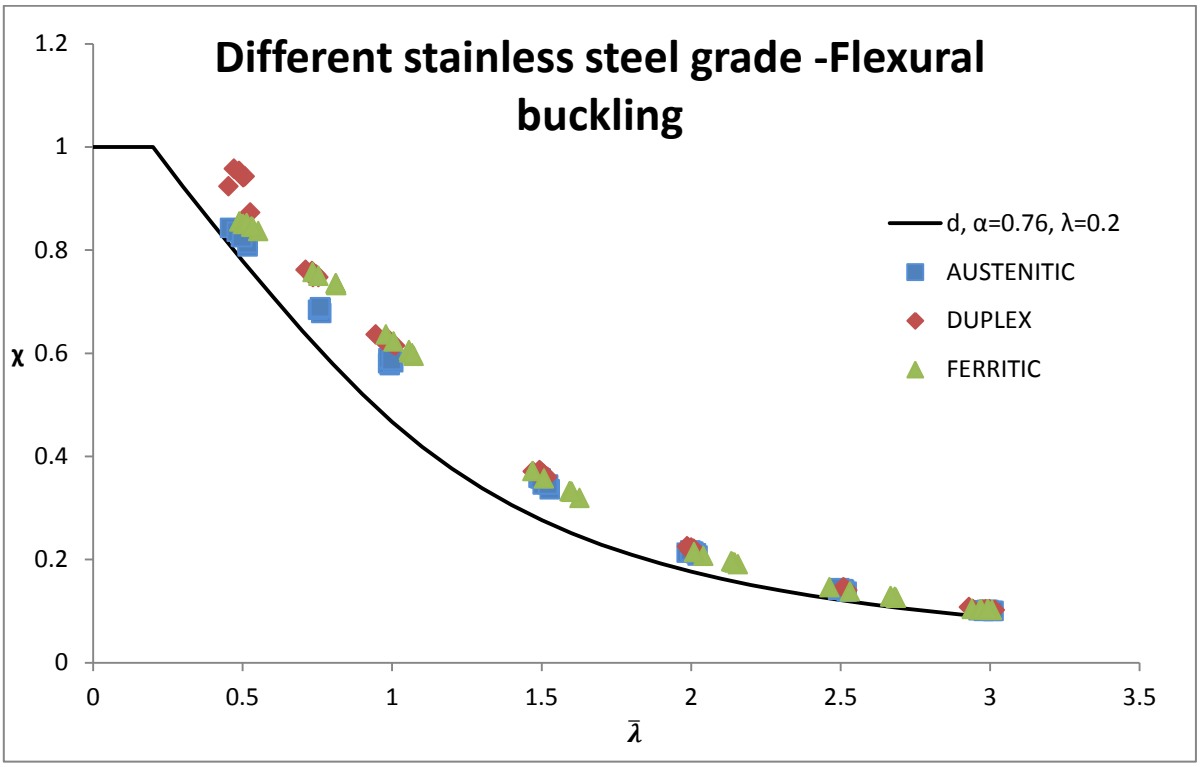

Figure 37. Assessment of the EN1993-1-4 (2006) buckling curve d for different stainless steel angle section members in compression

When observing Figure 37 in which all grades are represented it can be noticed that ferritic and duplex grades have a very similar behavior unlike austenitic grade which present for the same slenderness lower reduction factors, especially for low slenderness values.

This is due to the different stress-strain diagram shape of each material, while austenitic stainless steel has low yield stress, ferritic and duplex stainless steels have a considerably high yield stress. Therefore for the same load, austenitic grade could show a non-linear behavior, while the other two grades are still in the elastic branch. To analyze this subject and observe these differences between the materials a stress analysis has been made, where the failure stress (σ_f) have been plotted, for two different cross-sections, against their failure strain (ε_f).

This failure stress is approximated as P_u/A, and the failure stress is estimated from the material stress-strain curve, explained in the section 3.4.3 Material (parametric study).

In Table 17 the values of failure stress and strain for the sections 65x65x10 mm and 100x100x12 mm are shown, for the slenderness values 0.75 and 3 for all three different

grades. In Figure 38, the material characterization stress-strain curves are shown, where the failures of the different specimens have been identified.

Table 17. Stress analysis for three different slenderness values

Section	$\bar{\lambda}$	Grade	P_u (kN)	A (mm^2)	σ_f (MPa)	ε_f	Points
65x65x10	0.75	Austenitic	229.8	1200	192	0.00102	1
		Ferritic	287.9	1200	240	0.00121	
		Duplex	484.2	1200	403	0.00217	
100x100x12	0.75	Austenitic	434.3	2556	170	0.00087	2
		Ferritic	529.5	2556	207	0.00104	
		Duplex	893.3	2556	349	0.00179	
100x100x12	3	Austenitic	63.4	2556	25	0.00013	3
		Ferritic	74.2	2556	29	0.00015	
		Duplex	128.7	2556	50	0.00025	

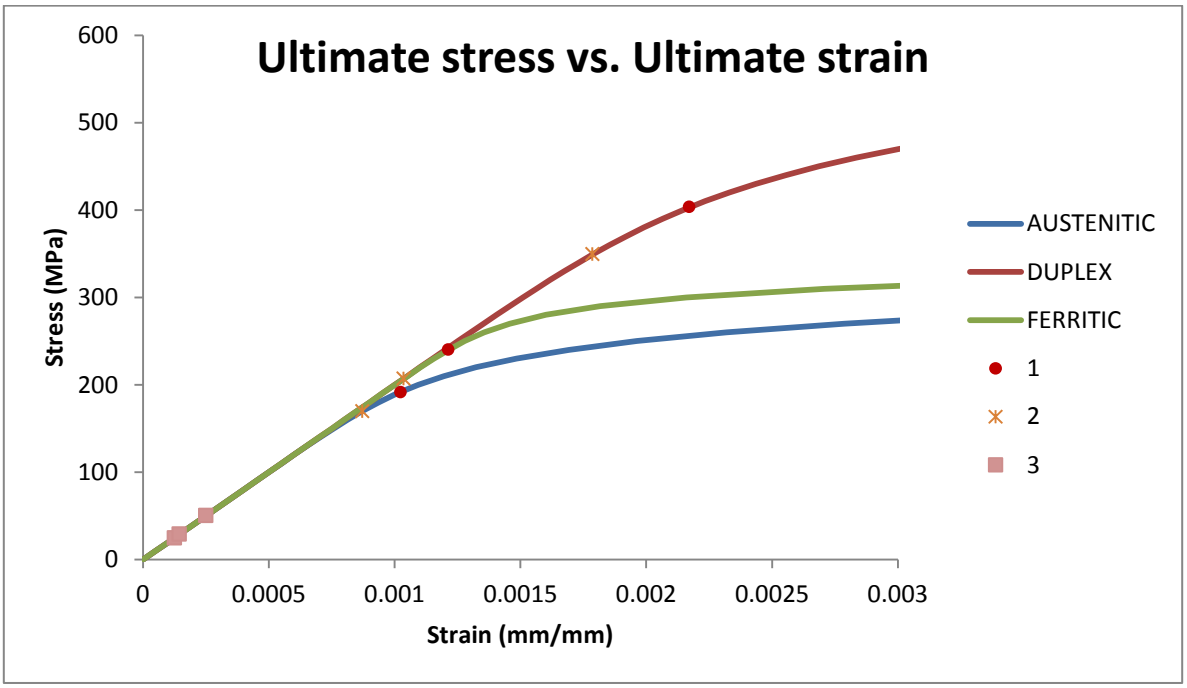

Figure 38. Ultimate stress vs. ultimate strain for different cases

As it can be seen in Figure 38, the points that were plotted were 1 and 2 that correspond to a non-dimensional slenderness of 0.75, where (as seen in Figure 37) this difference between the different grades is more notorious. Point 3 is also plotted in order to observe that with the increase of the slenderness the behavior for all grades gets very similar, especially because when a member is very slender, its failure will be due to instability instead of failing by their resistance.

When looking at Point 1 ($\bar{\lambda}$ =0.75 for member 65x65x10 mm) it can be noticed that for the moment when the ultimate load is reached the austenitic grade is already in the plastic branch and that its loss of stiffness is higher than the ferritic's and duplex's grades which are still in the elastic branch.

For Point 2 ($\bar{\lambda}$ =0.75 for member 100x100x12 mm) this same behavior is shown although austenitic grade is just entering into the plastic branch.

In brief, the differences between the austenitic grade and both the ferritic and duplex grades in low $\bar{\lambda}$ values (seen in Figure 37) are due to the to the difference in their proportionality limit when the ultimate load is reach, caused by their different behavior at low strains.

Finally, in order to confirm what has been showed in Figures 34, 35, 36 and 37, the mean of the ratio P_u/P_{Pred} (Mean) and the coefficient of variation (COV) are calculated for each material. In table 18 these values are presented for each material.

Table 18. Mean P_u/P_{Pred} ratios and COV for the buckling curve d

Austenitic	Mean	1.17
	COV	0.06
Ferritic	Mean	1.23
	COV	0.07
Duplex	Mean	1.23
	COV	0.05
ALL	Mean	1.21
	COV	0.07

The results shown in Table 18 confirm the evidence of the conservativeness of the curve d for the studied stainless steel columns, showing resistance underestimations of around 20%.

Expressions introduced in section 2.2.4.3 have been considered in this assessment and the partial safety factor (γ_{M1}) was taken equal to unity for comparison purposes.

For the sections that failed by flexural torsional buckling mode, the values $\bar{\lambda}$ vs χ_{FE} (FE) were plotted against the curve b (α=0.34, $\overline{\lambda_o}$=0.2), according to the established in EN1993-1-4 and DMSSS (2017), see Figures 39, 40 and 41.

In this case the slenderness for torsional-flexural buckling is determined as explained in 2.2.4.4, Eq. (11).

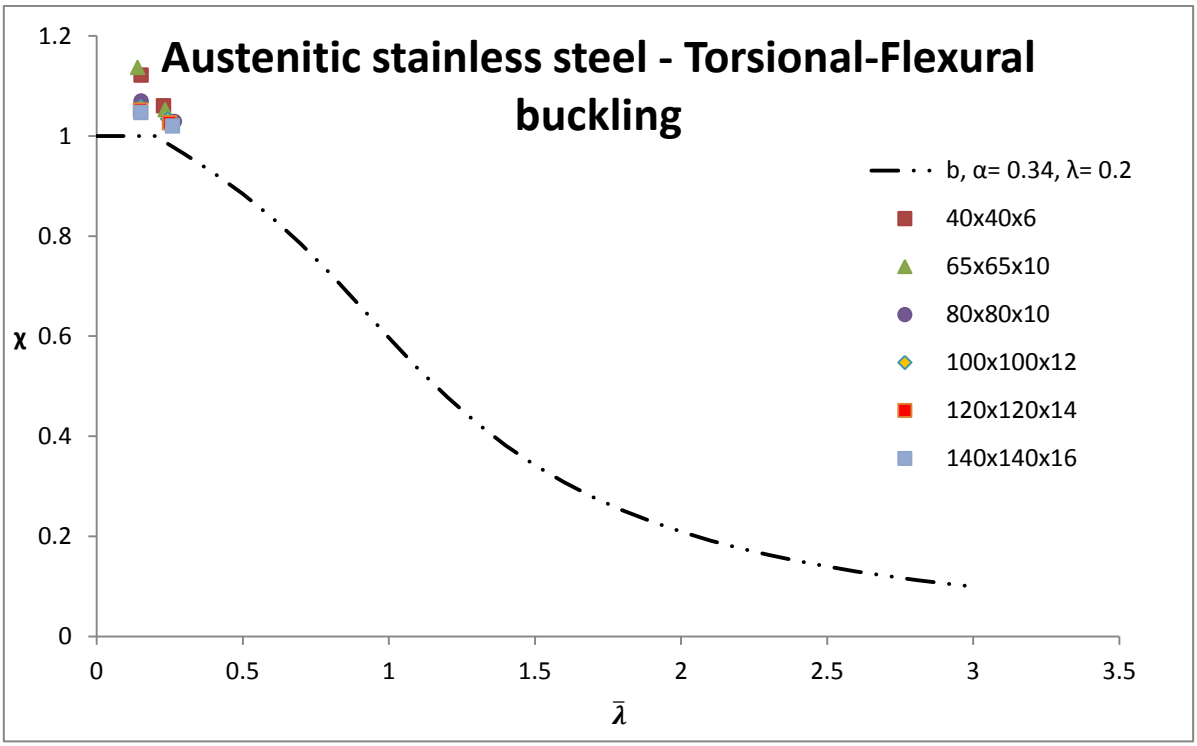

Figure 39. Assessment of the EN1993-1-4 (2006) buckling curve b for austenitic stainless steel angle section members in compression

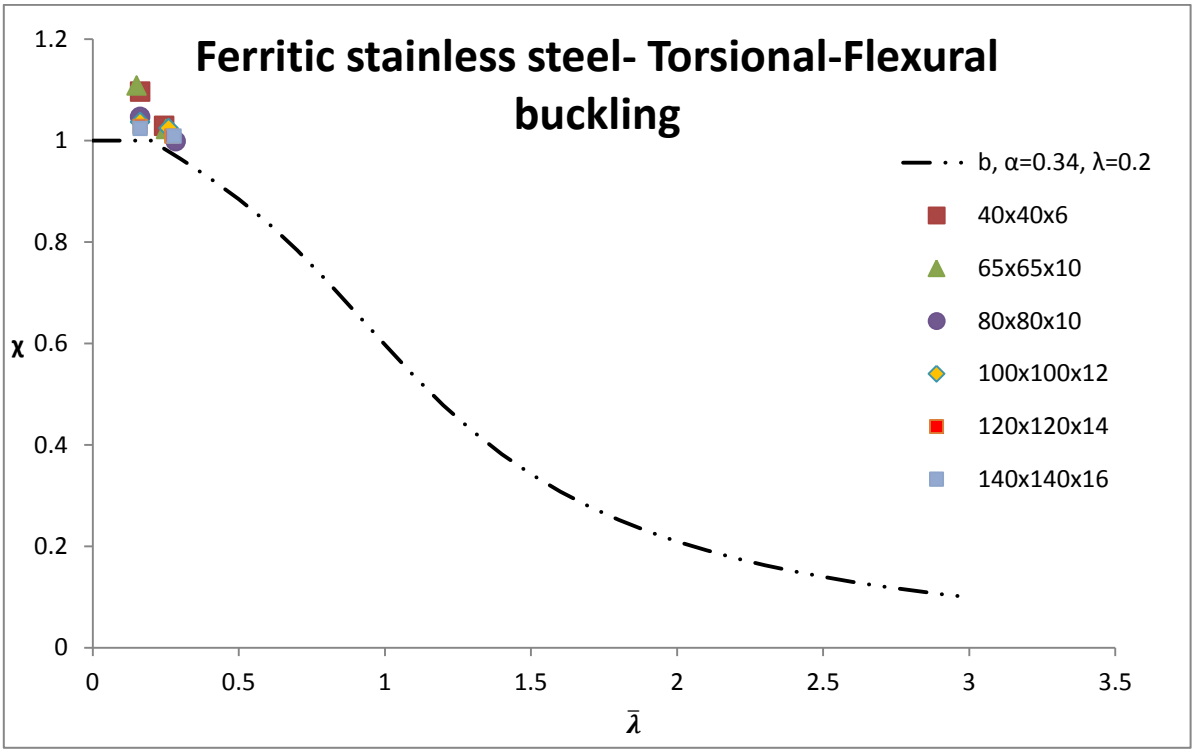

Figure 40. Assessment of the EN1993-1-4 (2006) buckling curve b for ferritic stainless steel angle section members in compression

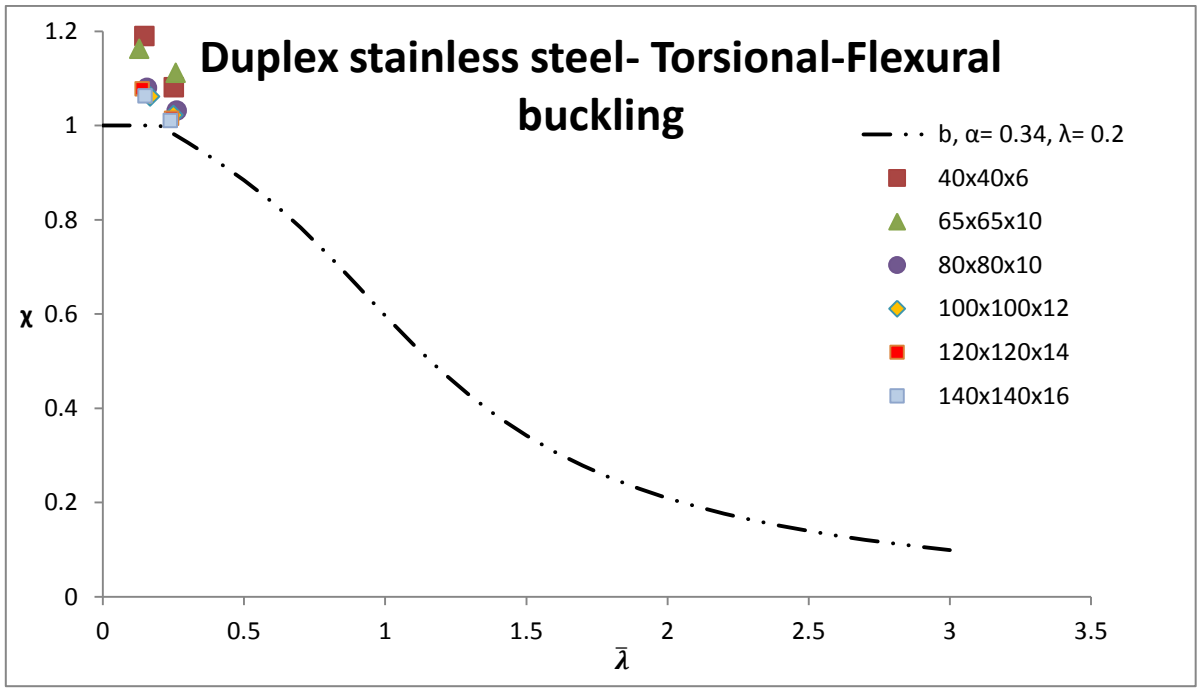

Figure 41. Assessment of the EN1993-1-4 (2006) buckling curve b for duplex stainless steel angle section members in compression

For the flexural torsional failure mode it can also be concluded that there is not difference between the different sections that were studied, the section does not influence the behavior of the member.

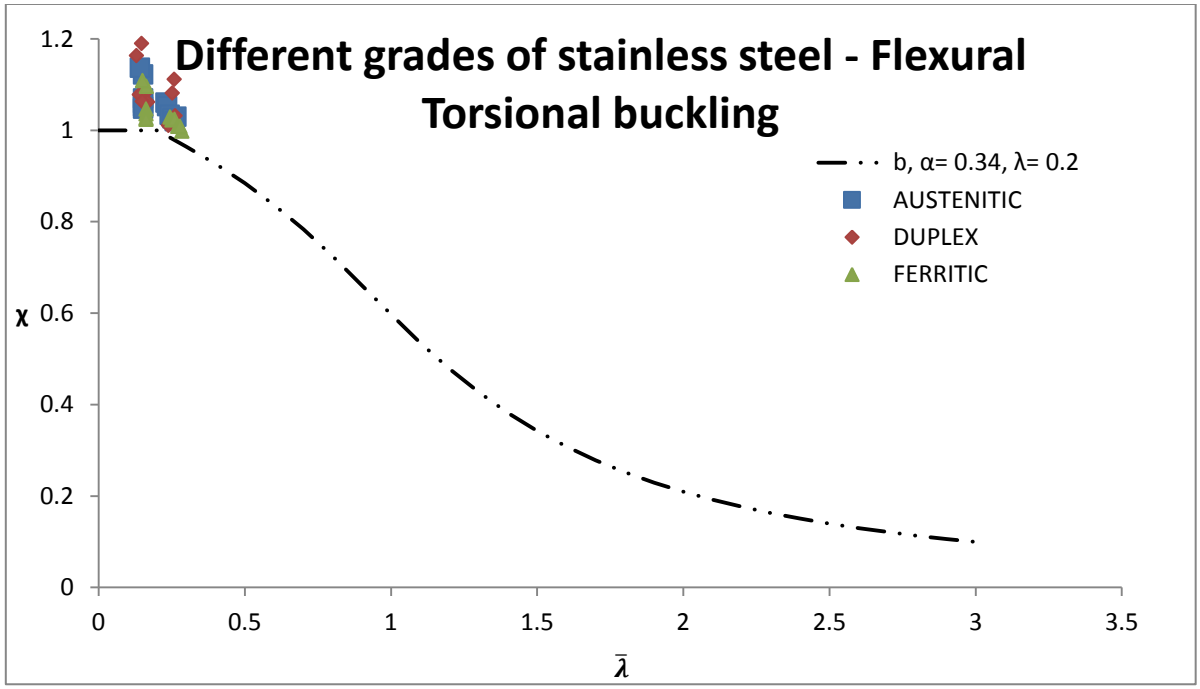

Figure 42. Assessment of the EN1993-1-4 (2006) buckling curve b for different stainless steel grades angle section members in compression

In this case, due to the high flexural stiffness of the cross-section the member is very susceptible to torsion (for short lengths) therefore they all fail trough flexural- torsional, and there is no difference between the grades, as shown in Figure 42.

Finally, in order to confirm what has been showed in Figures 39, 40, 41 and 42, the mean of the ratio P_u/P_{Pred} (Mean) and the coefficient of variation (COV) are calculated for each material. In Table 19 these values are presented for each material.

Table 19. Mean P_u/P_{Pred} ratios and COV for the buckling curve b

Austenitic	Mean	1.14
	COV	0.02
Ferritic	Mean	1.13
	COV	0.02
Duplex	Mean	1.22
	COV	0.02
ALL	Mean	1.16
	COV	0.04

In the results shown Figures 38, 39, 40, 41 and in Table 19 it can be observed that expressions and buckling curves currently given in EN1993-1-4 (2006) can be safely applied. However, these expressions have also been found to be overly conservative for the different stainless steel grades investigated in this study. Given the reduced number of columns failing in torsional-flexural buckling modes present in the database, and considering the low slenderness range covered (see Figure 42), it is considered that there is insufficient available data to propose alternative buckling curves for torsional-flexural buckling. Therefore, the following section investigates the applicability of alternative buckling curves only for the minor axis flexural buckling of stainless steel columns with angle sections based on the available data, providing a preliminary proposal.

5. DESIGN PROPOSAL

As was mentioned in the previous section (Behavior of stainless steel angle columns) the buckling curve proposed in the EN1993-1-4 for minor axis flexural buckling (curve d) is overly conservative for stainless steel angle columns. This can lead to an oversizing of the elements when designing and therefore to a non-efficient design. In this chapter a design proposal is presented, in order to improve this issue, by determining a less conservative curve to be used and perform a more efficient design.

5.1 Proposal

The results of the parametric study of flexural buckling are compared to all the buckling curves (curve b, c and d), in order to study which one of the curves is more appropriate and less conservative than the normative curve d, and could be used in the design of equal leg angle stainless steel members.

For all stainless steel grades (austenitic, ferritic and duplex), the comparisons with the buckling curves are made (curve b α=0.34, $\overline{\lambda_o}$=0.2, curve c α=0.49, $\overline{\lambda_o}$=0.2 and curve d α=0.76, $\overline{\lambda_o}$=0.2).This is achieved when calculating the mean of the ratio P_u/P_{Pred} (Mean) and the coefficient of variation (COV). In Table 20 these values are presented for each material.

Table 20. Mean of the ratio P_u/P_{Pred} (Mean) and the coefficient of variation (COV) for each material and each buckling curve

Buckling curve		**Curve d**	**Curve c**	**Curve b**
Austenitic	Mean	1.17	1.05	0.98
	COV	0.06	0.05	0.04
Ferritic	Mean	1.23	1.10	1.03
	COV	0.07	0.05	0.03
Duplex	Mean	1.23	1.11	1.03
	COV	0.05	0.03	0.03
ALL	Mean	1.21	1.09	1.02
	COV	0.07	0.05	0.07

As shown in Table 20 curve c and b for all the grades show a Mean value close to 1, and small coefficients of variation. This could lead to a good adjustment, however it is necessary to further study these curves in order to safely propose one of them.

In Figures 43, 44 and 45 the obtained values of member slenderness and reduction factor are plotted ($\bar{\lambda}$ vs χ_{FE} (FE) against the mentioned curves: curve b (α=0.34, $\overline{\lambda_o}$=0.2), curve c (α=0.49, $\overline{\lambda_o}$=0.2) and curve d (α=0.76, $\overline{\lambda_o}$=0.2).

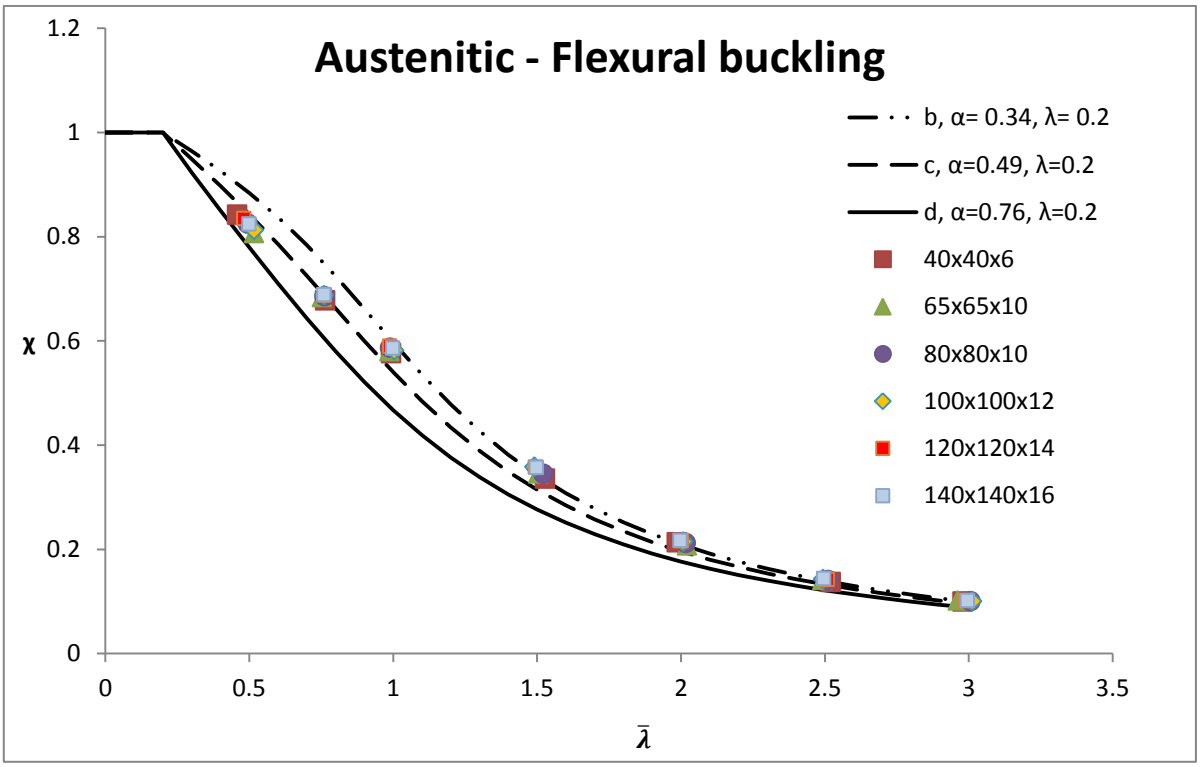

Figure 43. Comparison of obtained results for austenitic stainless steel against alternative buckling curves

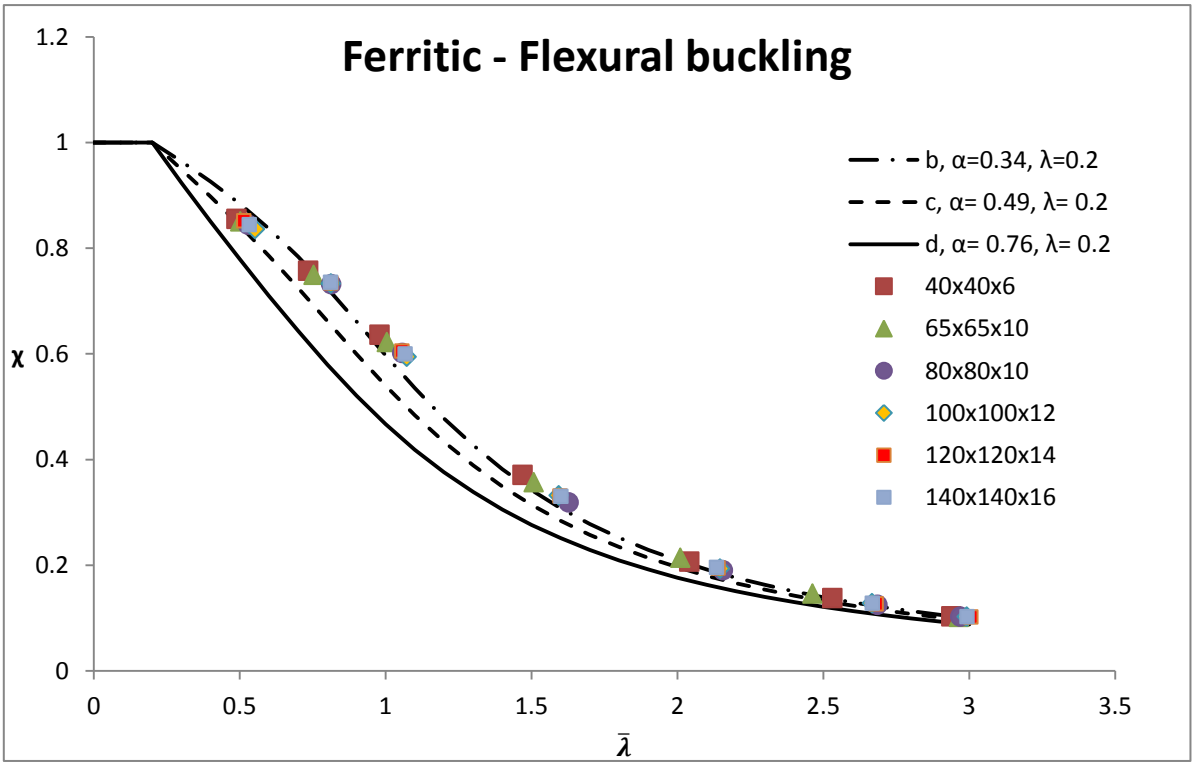

Figure 44. Comparison of obtained results for ferritic stainless steel against alternative buckling curves

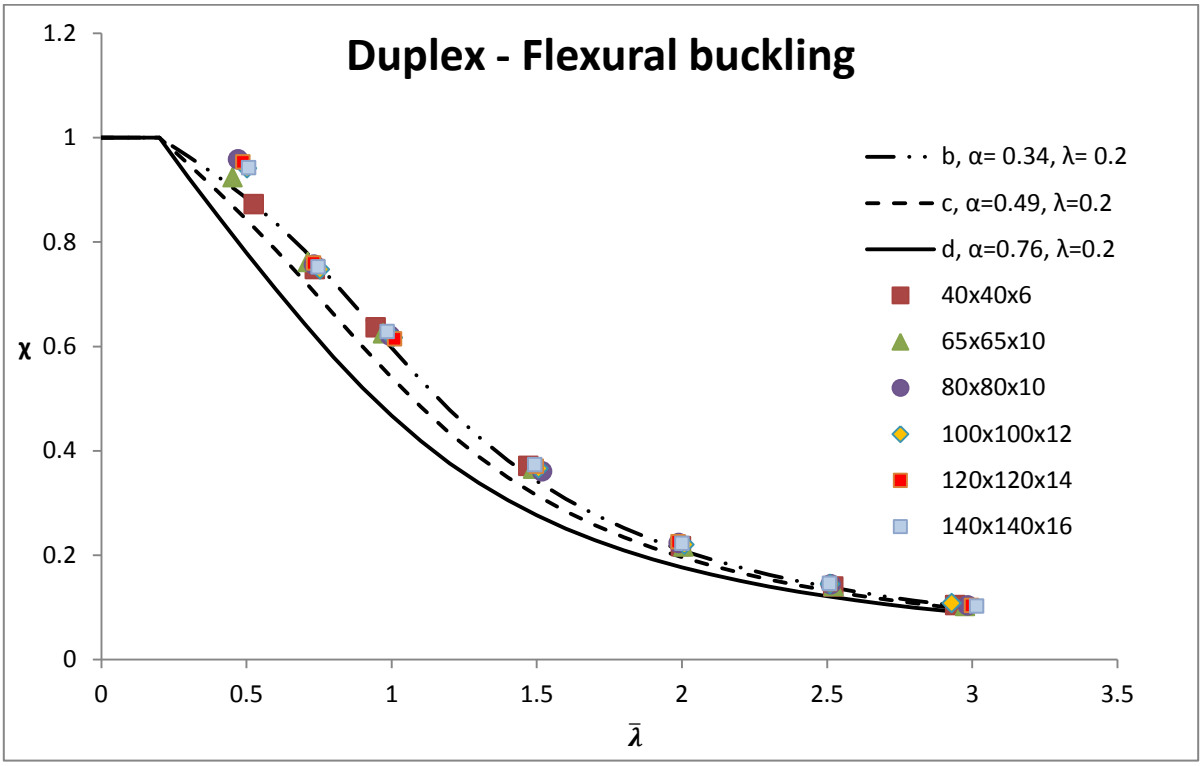

Figure 45. Comparison of obtained results for duplex stainless steel against alternative buckling curves

In order to evaluate the accuracy of the slenderness values and ultimate loads obtained in the parametric study, the ratio $N_{FE}/N_{b,pred}$ (where $N_{FE}=P_u$) is plotted against member slenderness ($\bar{\lambda}$) , this is made for all three stainless steel grades for each buckling curve, and is presented in Figures 46, 47 and 48.

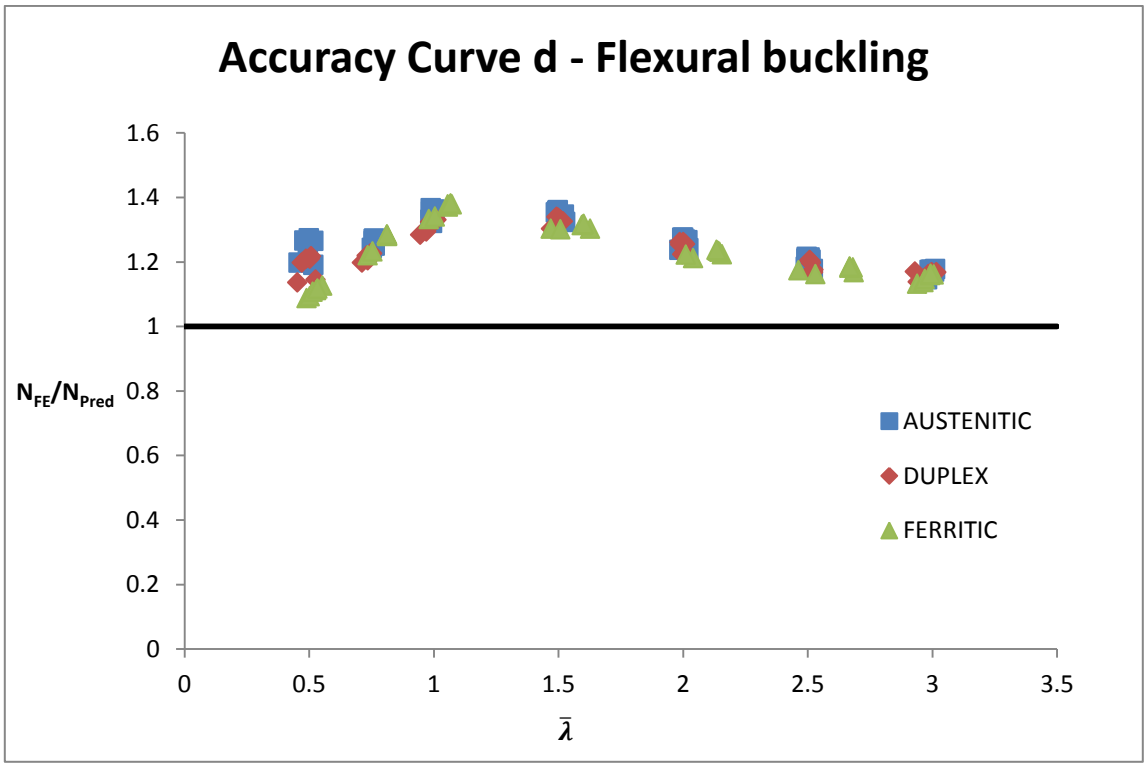

Figure 46. Accuracy of the obtained results for curve d EN1993-1-4

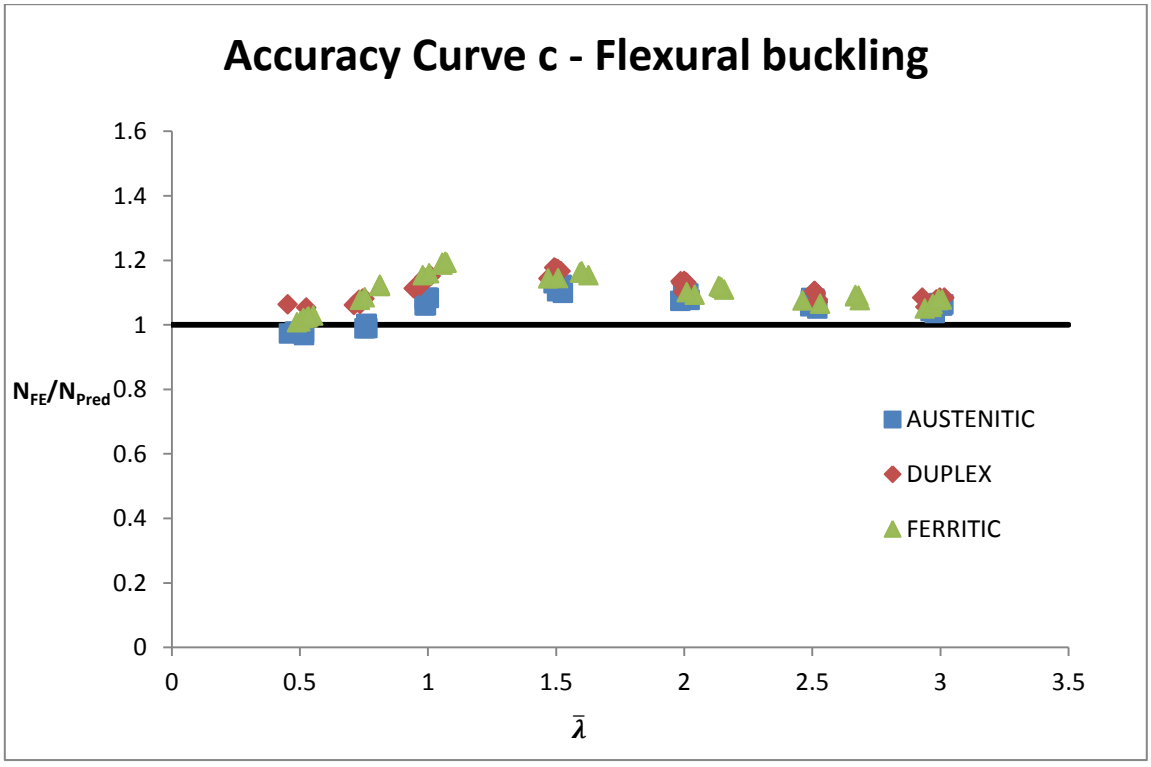

Figure 47. Accuracy of the obtained results for curve d EN1993-1-4

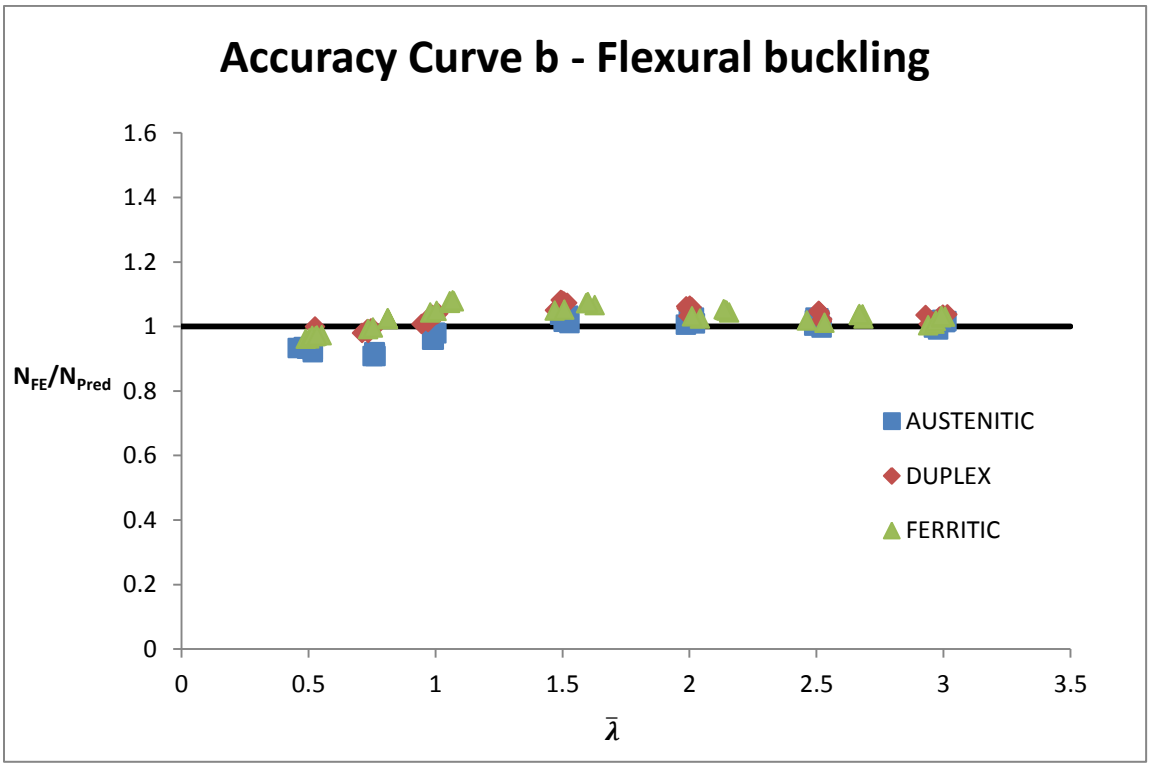

Figure 48. Accuracy of the obtained results for curve b EN1993-1-4

In Figure 46 it can be observe that for curve d all values remain on the conservative side, being all points above $N_{FE}/N_{Pred}=1$. For curve c (Figure 47) only a few values of austenitic grade are located under this line, showing that for a few cases curve c could be unsafe. Finally observing the Figure 48 for curve b many values of the austenitic, ferritic and a few of the duplex grade are under the value $N_{FE}/N_{Pred}=1$. Consequently curve b could also be unsafe for some cases.

After analyzing Table 20 and Figures 46, 47 and 48, the curve c is the proposed curve for flexural buckling when using equal leg single angle of stainless steel, because in general the obtained values seem to correctly adjust to this curve, being less conservative than the curve d, proposed in EN1993-1-4 (2006) for the studied case. Using curve c could lead to a safe design, without oversizing the members when designing.

In order to validate this proposal a reliability analysis is carried out in next section (5.2), in which the detailed steps needed to correctly execute this analysis are presented.

5.2 Reliability Analysis

The adopted design models carry deviations, as well as for the material and geometrical properties of all structural components, therefore as mentioned before, the design proposal must be validated, evaluating the partial resistance factor (γ_M), which must

include uncertainties in the mentioned properties (material, geometrical), but also imperfections and the design procedure itself (Tankova et al., 2014).

In order to validate the design proposal it is necessary to perform a reliability analysis. This is a statistical analysis and has been derived according to EN1990, Annex D (2005) specifications, to obtain the partial resistance factor for member resistance, accounting for model uncertainties and model variations.

The statistical parameters corresponding to the material and geometrical variations of the different stainless steel grades have been extracted from Afshan et al. (2015), where the COVs corresponding to the yield strength for stainless steel grades austenitic, ferritic and duplex are 0.060, 0.045 and 0.030 respectively, and the COV of the geometric properties was taken as 0.050.

This analysis is made for each considered buckling curve and for all 3 materials. First, it is necessary to identify the variables to follow the procedure established in the EN1900, Annex D (2005). The theoretical values are the ones obtained according to EN1993-1-4 (2006) ($r_t=N_{b,EC}$), and experimental values are the ones obtained through the FE analysis ($r_e=N_{FE}$).

Next, it is necessary to estimate the mean value correction factor b, as the "Least Squares" best-fit to the slope, given in Eq. (23).

$$b = \frac{\sum r_e * r_t}{\sum r_t^2} \tag{23}$$

The coefficient of variation of the errors is estimated as shown in Eq. (24). To obtain it, it is necessary to calculate the error term (δ_i) for each experimental or numerical value, determined from Eq. (25), and then calculate the variables Δ_i, $\bar{\Delta}$ and s_Δ^2 according to the Eqs. (26), (27) and (28) respectively.

$$V_\delta = \sqrt{exp(s_\Delta^2) - 1} \tag{24}$$

$$\delta_i = \frac{r_{ei}}{b * r_{ti}} \tag{25}$$

$$\Delta_i = \ln(\delta_i) \tag{26}$$

$$\bar{\Delta} = \frac{1}{n}\sum_{i=1}^{n} \Delta_i \tag{27}$$

$$s_\Delta^2 = \frac{1}{n-1}\sum_{i=1}^{n} (\Delta_i - \bar{\Delta})^2 \tag{28}$$

To take into account the variation of the material, the geometry and the model the coefficient of variation is calculated as shown in Eq. (29)

$$V_r^2 = \left(V_\delta^2 + 1\right)\left[\prod_{i=1}^{j}(V_{Xi}^2 + 1)\right] - 1 \tag{29}$$

The variability due to the FE modeling has also been included in the analysis, since some deviation between tests and the modeled reality was observed. For this, the coefficient of variation V_{FE} =0.028 has been included in the coefficient of variation V_{rt} that accounts for the sensitivity of the resistance function to the variability of the basic imput parameters. For this, the same procedure is followed, taking:

$$r_{ei} = r_{exp} \tag{30}$$

$$r_t = r_{FE} \tag{31}$$

Finally the design value of the resistance (r_d) should be obtained from Eq. (32)

$$r_d = b * g_{rt}(X_m)\exp(-k_{d,\infty} * \alpha_{rt} * Q_{rt} - k_{d,n} * \alpha_\delta * Q_\delta - 0.5 * Q^2) \tag{32}$$

Where:

$g_{rt,Xm}$ is the nominal value of the buckling load ($N_{b,EC}$).

$k_{d,n}$ is the design fractile factor, 3.04 for n>30

$k_{d,\infty}$ is the value for $k_{d,n}$ for $n\rightarrow\infty$ [$k_{d,\infty}$=3.04]

α_{rt} and α_δ are the weighting factor for Q_{rt} and Q_δ respectively, given in Eqs. (33) and (34), respectively.

Q_{rt}, Q_δ, Q are the standard deviation of the lognormal variables, given in Eqs. (35) and (36), respectively.

$$\alpha_{rt} = \frac{Q_{rt}}{Q} \tag{33}$$

$$\alpha_\delta = \frac{Q_\delta}{Q} \tag{34}$$

$$Q_{rt} = \sqrt{\ln(V_{rt}^2 + 1)} \tag{35}$$

$$Q_\delta = \sqrt{\ln\left(V_\delta^2 + 1\right)} \tag{36}$$

The nominal values of the yield strength are taken from the DMSSS, for the grades Austenitic (1.4301), Duplex (1.4462) and Ferritic (1.4003). These grades were chosen because of their wide and common use. In Table 21 these values are shown, where t is the thickness of the cross-section.

Table 21. Nominal values of the yield strength according to the thickness of the cross-section

Grade	t ≤ 8mm		t ≤ 13.5mm		t ≤ 75mm	
	f_y	f_u	f_y	f_u	f_y	f_u
Austenitic 1.4301	230	540	210	520	210	520
Ferritic 1.4003	280	450	280	450	250	450
Duplex 1.4462	500	700	460	700	460	640

Where:

f_y is the yield strength

f_u is the ultimate strength

Finally to obtain the corrected partial factor for resistances (γ_M) the Eqs. (37) and (38) are used.

$$\gamma_M = \frac{r_{t,nom}}{r_d} \tag{37}$$

$$\gamma_{M1} = \frac{\sum r_{ti,nom}^2}{\sum r_{t,nom} * r_d} \tag{38}$$

In Table 22 the summary and the results for the reliability analyses for each material and each curve are presented respectively. And in Table 23 the calculated partial safety factors are summarized.

Table 22. Summary and results for the reliability analyses for each material and each curve

Material	Curve	b	V_d	Vr
Austenitic	d	1.13	0.06	0.103
	c	1.02	0.05	0.096
	b	0.95	0.05	0.095
Ferritic	d	1.22	0.07	0.101
	c	1.09	0.05	0.087
	b	1.01	0.03	0.080
Duplex	d	1.24	0.05	0.082
	c	1.11	0.03	0.072
	b	1.02	0.03	0.070

Table 23. Calculated partial factors (γ_{M1}) with the reliability analysis for the design proposal according to Annex D in EN1990 (2005)

Material	Curve	γ_{M1}
Austenitic	d	1.013
	c	1.091
	b	1.161
Ferritic	d	1.036
	c	1.100
	b	1.154
Duplex	d	1.001
	c	1.089
	b	1.179

As shown in Table 23 it can be observe that the following expression is fulfilled:

$$\gamma_{calculated} \leq \gamma_{M1,EN}$$

Therefore, this analysis has validated the design proposal, which consists in using the curve c for the design of equal leg single angle of stainless steel. This validation through statistical analysis has been derived according to EN1990, Annex D (2005) specifications. Curve c has been also proven to correctly represent the failure modes for all members, as shown in Table 15, which also validates this proposal as it is safe when predicting how the specimen is going to fail.

6. CONCLUSIONS

When designing structures is very important to do it efficiently, regardless the considered construction material, in order to reduce costs and environmental impact.

This efficiency is mostly linked with the adopted structural typology and general design, which rely on the engineers and their capacity to search optimum solutions. However, the efficiency of a structure also depends on the design provisions codified in the different standards. In this case where the used material is stainless steel, efficient design becomes a determining factor, due to its high cost in comparison to carbon steel. With efficient design expressions that account for the non-linear stress-strain response and strain hardening effects, and the use of less conservative buckling curves for stainless steel, a more efficient, economic and sustainable structural design could be achieved.

In addition to this, and as presented in chapter 2 (Previous experimental programmes on angle section members) angle sections present a highly complicated structural behavior, and has not been studied as much as other open sections, furthermore the experimental programmes on stainless steel angle sections are even less common and experimental data is considerably limited. Consequently, the design standards of stainless steel are very conservative, specifically the flexural buckling curves for stainless steel in EN1993-1-4 (2006) and need to be revised.

Therefore, the main objective of this work was to understand the cross-sections and member behavior of stainless steel angle sections when subjected to pure compression, in order to gain knowledge as well as extend the limited numerical research about the behavior of angle section and propose alternative guidance. This alternative options would lead to a more efficient design methods that would lead to less tonnage use of the material for the same applied structural load levels, considerably reducing initial material costs and environmental impact.

To investigate the behavior of stainless steel angle sections a finite element (FE) model was developed using the general-purpose Software ABAQUS, and then validated with experimental data in the literature. Later, validated FE models were systematically utilized in order to perform parametric studies, presented in chapter 3, in order to identify the influence of the key parameters in the behavior of stainless steel angle sections and increase the amount of available data, considering three different stainless steel grades that were chosen because of their wide and common use, (Austenitic (1.4301), Duplex (1.4462) and Ferritic (1.4003)), 6 different cross-sections and 9 member slenderness. Therefore a total of 162 columns were studied, fulfilling the objective of this work: to study the structural behavior of equal-leg angle sections subjected to compression.

After analyzing the results in chapter 4 of the parametric study against the codified buckling curves in EN1993-1-4 it was determined that there is not difference between the different sections that were studied, therefore the behavior of the member does not depend on the dimensions of the cross-section for the chosen ranges. However, it was noticed that austenitic grade had a different behavior than ferritic and duplex grades, when

the members failed through flexural buckling for low non-dimensional slenderness. Therefore a stress analysis was made, in order to study the cause of this notorious difference and it was shown that it is mainly due to the to the difference in their stiffness when the ultimate load is reach, caused by their different behavior at low strains. This was observed when studying the failure stress and strain (when $\bar{\lambda}$ =0.75 for member 65x65x10 mm), because for the moment when the ultimate load was reached the austenitic grade was already in the plastic branch and that its stiffness was lower than the ferritic's and duplex's grades which were still in the elastic branch.

For the members that failed through flexural-torsional buckling it was observed that there was no difference between the grades, unlike for flexural buckling, because of the low stiffness of the cross-section that makes members very susceptible to torsion for short lengths. After analyzing the results of the flexural-torsional buckling it was observed that the stipulated buckling curve for torsional-flexural buckling (curve b) according to the EN1993-1-4 is adequate.

One of the main conclusions when analyzing the obtained results was that the stipulated buckling curve for flexural buckling (curve d) according to the EN1993-1-4 is very conservative and may be leading to an oversizing of the elements when designing.

Consequently in chapter 5 curve c was proposed for flexural buckling as a design proposal, after analyzing all the obtained results and comparisons with the codified curves in EN1993-1-4, being this curve less conservative than the one stipulated. Curve c has been also proven to correctly represent the failure modes for all members, which could validate this proposal as it is safe when predicting how the specimen is going to fail. However, a reliability analysis was performed in order to validate this proposal. This consisted in a statistical analysis derived from to EN1990, Annex D (2005) specifications. After determining that: $\gamma_{calculated} \leq \gamma_{M1,EN}$ the proposal was validated.

6.1 Suggestions for future research

The suggestions for future research have emerged from the development of this work and are proposed in this last section.

First of all it is necessary to reinforce this study with more numerical models and experimental tests if possible, in order to increase even more the reduced available data regarding the structural behavior of stainless steel angle sections.

Secondly, in order to complete this subject it would be recommendable to study this structural behavior for class 4 sections to see how this could affect the study.

Also, a study could be made to analyze the interaction between different types of buckling.

Finally, extend the analysis to cold-formed sections or different-leg angle sections.

7. REFERENCES

ABAQUS. (2012). ABAQUS/Standard user's manual volumes I-III and ABAQUS CAE manual. Version 6.12. Hibbitt, Karlsson & Sorensen, Inc., Pawtucket, USA.

Afshan, S., Zhao, O. and Gardner, L. (2017). Standardised Material Properties for Numerical Parametric Studies of Structural Stainless Steel Elements. Proceedings of the Fifth International Experts Seminar in Stainless Steel in Structures. London, UK.

AISC. (2005). Specification for Structural Steel Buildings. American Institute of Steel Construction Chicago, IL, USA.

AISI. (1974). American Iron and Steel Institute, Specification for the design of cold-formed stainless steel structural members, Washington, D.C., 1974.

Arrayago, I. (2016). New approach for efficient design of stainless steel RHS and SHS elements. Doctoral Thesis. Universitat Politècnica de Catalunya.

Arrayago, I., Real, E. and Gardner, L. (2015). Description of stress-strain curves for stainless steel alloys. *Materials and Design*, 87, 540–552.

AS/NZS4673. (2001). Cold-formed stainless steel structures. Sydney: Standards Australia; 2001.

Becque, J. and Rasmussen, K. J. R. (2006). Experimental Investigation of the Interaction of Local and Overall Buckling of Cold-Formed Stainless Steel Columns. Research Report No R873. Centre for Advanced Structural Engineering, School of Civil Engineering, The University of Sydney.

Becque, J. and Rasmussen, K. J. R. (2008). Numerical Investigation and Design Methods for Stainless Steel Columns failing by Interaction of Local and Overall Buckling. Research Report No R888. Centre for Advanced Structural Engineering, School of Civil Engineering, The University of Sydney

Bleich, F. (1952). Buckling Strength of Metal Structures. McGraw-Hill, New York.

Dinis, P.B., Camotim, D. and Silvestre, N. (2012). On the mechanics of thin-walled angle column instability. *Thin-Walled Structures,* 52, 80-89.

Dobrić, J. (2017). Evaluation of buckling curves – FE study. Research Report. Faculty of Civil Engineering, University of Belgrad.

Engesser, F. (1889). Zeitschrift fur Architektur und Ingenieurwesen. 35:455.

Euro Inox (1994). Design Manual for Stainless Steel. Second Edition.

Euro Inox (2007). Design Manual for Stainless Steel. Third Edition.

Euro Inox (2007). Design Manual for Stainless Steel. Third Edition. Commentary.

European Committee for Standardization. (2005). EN 1990. European Committee for Standardization Eurocode. Basis of structural design. Brussels, Belgium.

European Committee for Standardization. (2005). EN 1993-1-1. European Committee for Standardization Eurocode 3. Design of steel structures. Part 1-1: General rules and rules for buildings.Brussels, Belgium.

European Committee for Standardization. (2006). EN 1993-1-4. European Committee for Standardization Eurocode 3. Design of steel structures. Part 1-4: General rules. Supplementary rules for stainless steel. Brussels, Belgium.

Gardner, L. and Ashraf, M. (2006). Structural design for non-linear metallic materials. *Engineering Structures,* 28 (6), 926-934

Gardner, L., Insausti, A., Ng, K.T and Ashraf, M. (2010). Elevated temperature material properties of stainless steel alloys. *Journal of Constructional Steel Research*, 66 (5), 634-647.

Hradil, P., Talja, A., Real, E., Mirambell, E. and Rossi, B. (2013). Generalized multistage mechanical model for nonlinear metallic materials. *Thin-Walled Structures,* 63, 63-69.

Jain, A. and Rai, D. C. (2014). Lateral-torsional buckling of laterally unsupported single angle sections loaded along geometric axis. *Journal of Constructional Steel Research*, 102, 178–189.

Jandera, M. and Zhang, W. (2017). Angles in compression. Research Report. Faculty of Civil Engineering, Czech Technical University in Prague.

Johnson, A. and Winter, G. (1966). Behaviour of Stainless Steel Columns and Beams. *Journal of Structural Engineering, American Society of Civil Engineers, ASCE* 92(ST5): 97-118.

Kettler, M., Taras, A. and Unterweger, H. (2017). Member capacity of bolted steel angles in compression – Influence of realistic end supports. *Journal of Constructional Steel Research*, 130, 22–35.

Landesmann A., Camotim D., Dinis P. and Cruz R. (2017). Short-to-intermediate slender pin-ended cold-formed steel equal-leg angle columns: Experimental investigation, numerical simulations and DSM design. *Engineering Structures,* 132, 471-493.

Maia W., Vieira L., Schafer B. and Malite M. (2016). Experimental and numerical investigation of cold-formed steel double angle members under compression. *Journal of Constructional Steel Research,* 121, 398-412.

Menezes, A. A. De, Pedro, C. G., Vellasco, S., Lima, L. R. O. De and André, T. (2017). An Investigation of Austenitic Stainless Steel Hot Rolled Angle Sections under Axial Compression. Proceedings of the Fifth International Experts Seminar in Stainless Steel in Structures. London, UK.

Ministerio de Fomento. (2012). EAE, Instrucción de Acero Estructural. Third Edition.

Mirambell, E. and Real, E. (2000). On the calculation of deflections in structural stainless steel beams: an experimental and numerical investigation. *Journal of Constructional Steel Research,* 54 (4), 109-133.

Popovic, D., Hancock, G.J. and Rasmussen, K.J.R. (1999). Axial compression tests of cold-formed angles. *Journal of Structural Engineering,* 125(5), 515-523

Quach, W.M., Teng, J.G. and Chung, K.F. (2008). Three-stage full-range stress-strain model for stainless steels. *Journal of Structural Engineering ASCE,* 134 (9), 1518-1527.

Rasmussen, K.J.R. (2003). Full-range stress-strain curves for stainless steel alloys. *Journal of Constructional Steel Research,* 59 (1), 47-61.

Rasmussen, K.J.R. (2005). Design of angle columns with locally unstable legs. *Journal of Structural Engineering ASCE,* 131(10), 1553-1560.

Rasmussen, K.J.R., Burns, T., and Bezkorovainy, P. (2004). Design of Stiffened Elements in Cold-Formed Stainless Steel Sections. *Journal of Structural Engineering,* 130(11), 1764-1771.

SEI/ASCE 8-02. (2002). Specification for the design of cold-formed stainless steel structural members. American Society of Civil Engineers (ASCE), Reston, US, 2002.

Shanley, F. (1947). Inelastic Column Theory. *Journal of Aeronautical Sciences*, 14(5), 261-276.

Shifferaw, Y. and Schafer, B. W. (2014). Thin-Walled Structures Cold-formed steel lipped and plain angle columns with fixed ends. *Thin-Walled Structures,* 80, 142–152.

Steel Construction Institute (2017). Design Manual for Stainless Steel. Fourth Edition.

Stowell, E. (1948). A Unified Theory of Plastic Buckling of Columns and Plates. Technical Note No. 1556. National Advisory Committee for Aeronautics, Washington, DC.

Trahair, N.S. (2002). Moment capacities of steel angle sections. *Journal of Structural Engineering ASCE* 128(11), 1387-1393.

Trahair, N.S. (2005). Buckling and torsion of steel unequal angle beams. *Journal of Structural Engineering ASCE* 131(3), 467-473.

Young, B., Silvestre, N., Camotim, D. and Asce, M. (2013). Cold-Formed Steel Lipped Channel Columns Influenced by Local-Distortional Interaction : Strength and DSM Design. *Journal of Structural Engineering,* 139(6), 1059–1074.

Young, B. (2004). Tests and design of fixed-ended cold-formed steel plain angle columns. *Journal of Structural Engineering ASCE,* 128(11), 1394-1398.

Young, B. and Chen, J. (2008). Column tests of cold-formed steel non-symmetric lipped angle sections. *Journal of Constructional Steel Research,* 64, 808–815.

Young, B. and Ellobody, E. (2005). Finite element analysis of cold-formed steel lipped angle compression members. *Advances in Steel Structures*, I, 469–478.